Electronic Supplementary Material (ESI) for Organic & Biomolecular Chemistry.

Supporting Information

Table of contents **Page**

1. General

Column chromatography was carried out with silica gel 60 (particle size 0.040-0.063 mm, 230-400 mesh) and commercially available solvents. Thin-layer chromatography (TLC) was conducted on aluminium sheets coated with silica gel 60 F254 with visualization by a UV lamp (254 or 360 nm). Melting points (m.p.) were measured in open capillaries and were uncorrected. ^{1}H and ^{13}C NMR spectra were recorded at 400/500 and 100/125 MHz at 25 °C with a Bruker AVANCE III 400/500 instruments equipped with BBO/Prodigy cryoprobe. Chemical shifts are reported in ppm relative to the signal of Me_4Si. The residual solvent signal in the ^{1}H and ^{13}C NMR spectra was used as an internal reference ($CDCl_3$ 7.25 and 77.23 ppm). Apparent resonance multiplicities are described as s (singlet), br s (broad singlet), d (doublet), and m (multiplet). Due to limited solubility of target compounds (especially **B7**), some signals of the quaternary carbons were not observed in ^{13}C NMR spectra. ^{1}H signals of 1,4-phenylene moieties were denoted as Ph. IR spectra were recorded as neat using HATR adapter on a Perkin-Elmer FTIR Spectrum BX spectrometer. EI-MS spectra were measured on a GC/MS configuration comprised of an Agilent Technologies 6890N gas chromatograph equipped with a 5973 Network MS detector (EI 70 eV, mass range 33–550Da). High resolution MALDI MS spectra were measured on a MALDI mass spectrometer LTQ Orbitrap XL (Thermo Fisher Scientific, Bremen, Germany) equipped with nitrogen UV laser (337 nm, 60 Hz). The LTQ Orbitrap instrument was operated in positive-ion mode over a normal mass range (*m/z* 50 - 1500) with the following setting of tuning parameters: resolution 100,000 at *m/z* = 400, laser energy 17 mJ, number of laser shots 5, respectively. The survey crystal positioning system (survey CPS) was set for the random choice of shot position by automatic crystal recognition. The isolation width $\Delta m/z$ 4, normalised collision energy 25%, activation Q value 0.250, activation time 30 ms and helium as

the collision gas were used for CID experiments in LTQ linear ion trap. The used matrix was 2,5-dihydroxybenzoic acid (DHB). Mass spectra were averaged over the whole MS record (30 s) for all measured samples. The absorption spectra were measured on a Perkin Elmer Lambda 35 UV/VIS Spectrophotometer. The fluorescence spectra were measured on Perkin Elmer LS 55 Spectrofluorimeter. As the fluorescence bands of the investigated compounds are located in a broad wavelength range (450-800 nm), DCM in *n*-propanol (λ_{max}^{F} = 614 nm, q_F = 0.57)[1] and coumarin 153 in ethanol (λ_{max}^{F} = 536 nm, q_F = 0.38)[2] were used as standards for the determination of the fluorescence quantum yields. Elemental analyses were performed on an EA 1108 Fisons instrument

2. Synthesis of intermediates

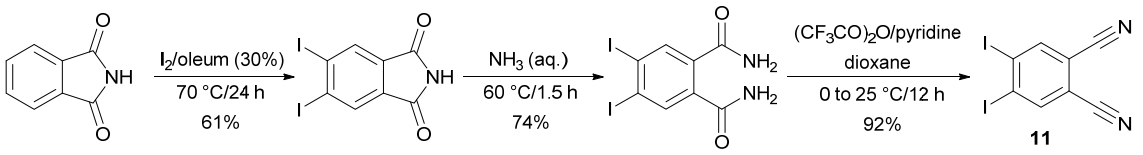

Scheme S1 Synthetic path to 4,5-diiodobenzene-1,2-dicarbonitrile **11**.

4,5-Diiodophthalimide

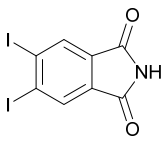

A mixture of oleum (30 ml, 30%), phthalimide (20 g, 0.14 mol) and I2 (34.5 g, 0.14 mol) was stirred and heated at 70 °C for 24 h. The resulting suspension was poured over ice, the precipitate was filtered, washed with water (2 × 75 ml), 2% aq. K_2CO_3 (50 ml) and aq. Na_2SO_3 (50 ml). The crude product was recrystallized from acetone/water to give 34 g (61 %) of title compound as an off-white solid. M.p. 267–269 °C (Ref.[3] m. p. 297–299 °C). ^{1}H-NMR (400 MHz, 25 °C, d_6-DMSO): δ_H = 11.5 (s, 1H, NH), 8.31 ppm (s, 2H, ArH). ^{13}C-NMR (100 MHz, 25 °C, d_6-DMSO): δ_C = 167.8, 133.04, 132.71, 116.57 ppm. EI-MS (70 eV)

m/z (rel. int.): 399 (100, M^+), 355 (8), 229 (15), 201(10), 74 (10). HR-FT-MALDI-MS (DHB) *m/z*: 399.8340 ($[M+H]^+$), $C_8H_4I_2NO_2^+$ requires 399.8326.

4,5-Diiodophthaldiamide

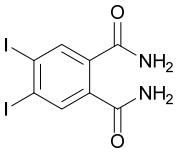

A mixture 4,5-diiodophthalimide (5.3 g, 13.0 mmol) and aq. NH_3 (58 ml, 25%) was stirred and heated at 60 °C for 1.5 h. The resulting suspension was filtered, the precipitate was washed with cold water (3 × 50 ml), methanol (50 ml) and air-dried to give 4.1 g (74 %) of title compound as a white solid. M.p. 294–296 °C (Ref.[1] m.p. 297–299 °C). ^{1}H-NMR (400 MHz, 25 °C, d_6-DMSO): δ_H = 7.97 (s, 2H, ArH), 7.88 (s, 2H, NH_2), 7.46 ppm (s, 2H, NH_2). ^{13}C-NMR (100 MHz, 25 °C, d_6-DMSO): δ_C = 167.91, 137.61, 137.07, 109.94 ppm. HR-FT-MALDI-MS (DHB) *m/z*: 416.8607 ($[M+H]^+$), $C_8H_7I_2N_2O_2^+$ requires 416.8591.

4,5-Diiodobenzene-1,2-dicarbonitrile (11)

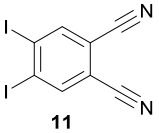

11

Trifluoroacetic anhydride (21.2 ml, 0.15 mol) was added dropwise to a mixture of 4,5-diiodophthaldiamide (11 g, 0.026 mol), dioxane (110 ml) and pyridine (24 ml) at 0–5 °C. The resulting suspension was stirred at 25 °C for 12 h, poured over ice and extracted with ethyl acetate (3 × 100 ml). The combined organic extracts were washed with water (50 ml), 1M HCl (55 ml), aq. Na_2CO_3 (150 ml), water (50 ml) and dried (Na_2SO_4). The solvents were evaporated *in vacuo* and the residue was crystallized from acetone/water to give 9.2 g (92 %) of title compound as an off-white solid. M.p. 214–216 °C (Ref.[1] m.p. 216-217 °C). ^{1}H-NMR (400 MHz, 25 °C, $CDCl_3$): δ_H = 8.21 ppm (s, 2H, ArH). ^{13}C-NMR (100 MHz, 25 °C, $CDCl_3$): δ_C = 142.87, 115.55, 115.32, 113.8 ppm. EI-MS (70 eV) *m/z* (rel. int.): 380 (100, M^+), 253 (30), 126 (20), 75 (10). HR-FT-MALDI-MS (DHB) *m/z*: 416.8607 ($[M+H]^+$), $C_8H_7I_2N_2O_2^+$ requires 416.8591.

3. Crystallography

The X-ray data for coloured crystals of chromophores **B1** and **B4** were obtained at 150K using Oxford Cryostream low-temperature device on a Nonius KappaCCD diffractometer with MoK_α radiation (λ = 0.71073 Å), a graphite monochromator, and the ϕ and χ scan mode. Data reductions were performed with DENZO-SMN.[4] The absorption was corrected by integration methods.[5] Structures were solved by direct methods (Sir92)[6] and refined by full matrix least-square based on F^2 (SHELXL97).[7] Hydrogen atoms were mostly localized on a difference Fourier map, however to ensure uniformity of the treatment of the crystal, all hydrogen atoms were recalculated into idealized positions (riding model) and assigned temperature factors $H_{iso}(H) = 1.2\ U_{eq}$(pivot atom) or of $1.5U_{eq}$ for the methyl moiety with C-H = 0.96, 0.97, and 0.93 Å for methyl, methylene and hydrogen atoms on sp^2 carbon atoms, respectively.

$R_{int} = \sum |F_o^2 - F_{o,mean}^2| / \sum F_o^2$, GOF = $[\sum(w(F_o^2 - F_c^2)^2)/(N_{diffrs} - N_{params})]^{½}$ for all data, $R(F) = \sum ||F_o| - |F_c|| / \sum |F_o|$ for observed data, $wR(F^2) = [\sum(w(F_o^2 - F_c^2)^2)/(\sum w(F_o^2)^2)]^{½}$ for all data.

Crystallographic data for structural analysis have been deposited with the Cambridge Crystallographic Data Centre, CCDC no. 984736 and 984735 for **B1** and **B4**, respectively. Copies of this information may be obtained free of charge from The Director, CCDC, 12 Union Road, Cambridge CB2 1EY, UK (fax: +44-1223-336033; e-mail: deposit@ccdc.cam.ac.uk or www: http:// www.ccdc.cam.ac.uk).

Crystallographic data for **B1**: (formula unit is formed by one molecule of **B1** and one molecule of chloroform): $C_{41}H_{31}Cl_3N_4$, M = 686.05, monoclinic, *Cc*, *a* = 38.9202(4), *b* = 12.3160(3), *c* = 14.8423(6) Å, β = 99.601(4) °, Z = 8, V = 7014.9(3) $Å^3$, D_c = 1.299 $g.cm^{-3}$, μ = 0.297 mm^{-1}, T_{min}/T_{max} = 0.929/0.963; $-49 \le h \le 49$, $-15 \le k \le 15$, $-18 \le l \le 17$; 51501 reflections measured (θ_{max} = 27 °), 14610 independent (R_{int} = 0.0648),

10843 with $I > 2\sigma(I)$, 865 parameters, S = 1.168, $R1$(obs. data) = 0.0763, $wR2$(all data) = 0.1622; max., min. residual electron density = 0.797, -0.452 eÅ^{-3}.

Crystallographic data for **B4**: (formula unit is formed by one molecules of **B4** and one molecule of chloroform): $C_{49}H_{46}Cl_2N_8$, M = 817.84, triclinic, *P*-1, *a* = 12.1480(5), *b* = 13.7149(6), *c* = 14.8781(12) Å, α = 98.900(6), β = 107.234(5), γ = 108.859(4) °, *Z* = 2, V = 2152.7(3) Å^3, D_c = 1.262 g.cm^{-3}, μ = 0.196 mm^{-1}, T_{min}/T_{max} = 0.934/0.964; -15 ≤ h ≤ 15, -17 ≤ k ≤ 17, -19 ≤ l ≤ 19; 43783 reflections measured (θ_{max} = 27.5 °), 9765 independent (R_{int} = 0.0298), 7658 with $I > 2\sigma(I)$, 532 parameters, S = 1.084, $R1$(obs. data) = 0.0513, $wR2$(all data) = 0.1166; max., min. residual electron density = 1.095, -1.003 eÅ^{-3}.

4. Electrochemistry

Electrochemical measurements were carried out in *N*,*N*-dimethylformamide containing 0.1 M Bu_4NPF_6 in a three electrode cell by cyclic voltammetry (CV) and rotating disc voltammetry (RDV). The working electrode was platinum disc (2 mm in diameter) for CV and RDV experiments. As the reference and auxiliary electrodes were used saturated calomel electrode (SCE) separated by a bridge filled with supporting electrolyte and Pt wire, respectively. All potentials are given *vs.* SCE. Voltammetric measurements were performed using a potentiostat PGSTAT 128N (AUTOLAB, Metrohm Autolab B.V., Utrecht, The Netherlands) operated via NOVA 1.10 software.

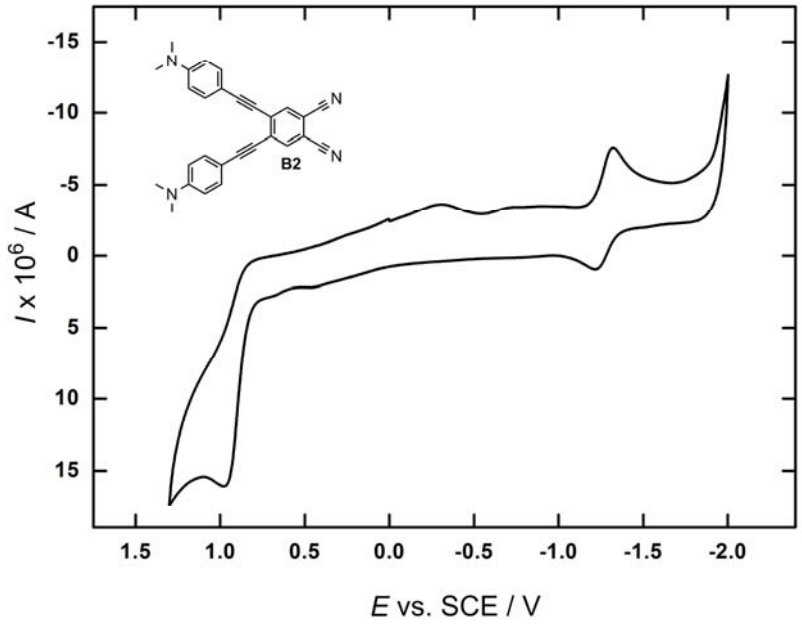

Fig. S1 Representative CV curve of the oxidation and reduction of compound **B2** at Pt electrode in DMF containing 0.1 M Bu_4NPF_6.

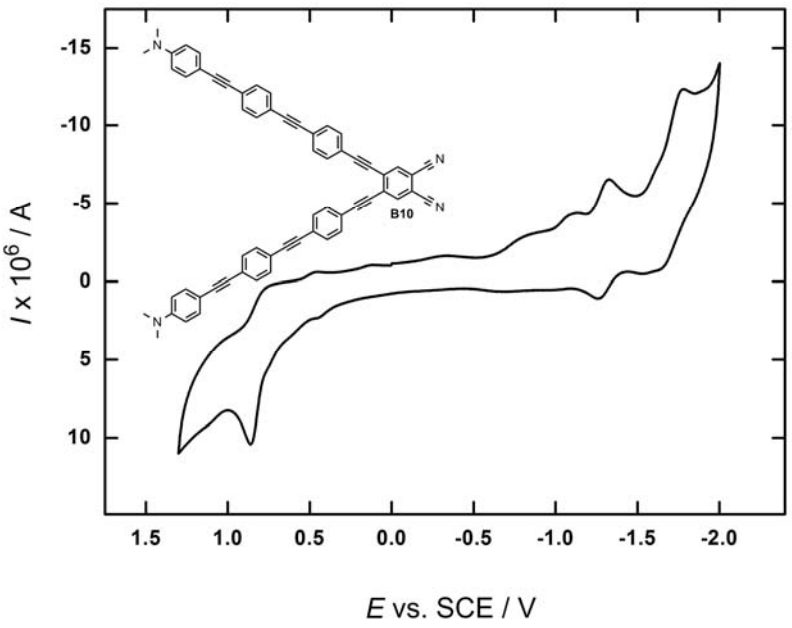

Fig. S2 Representative CV curve of the oxidation and reduction of compound **B10** at Pt electrode in DMF containing 0.1 M Bu_4NPF_6.

5. UV-Vis absorption and emission spectra

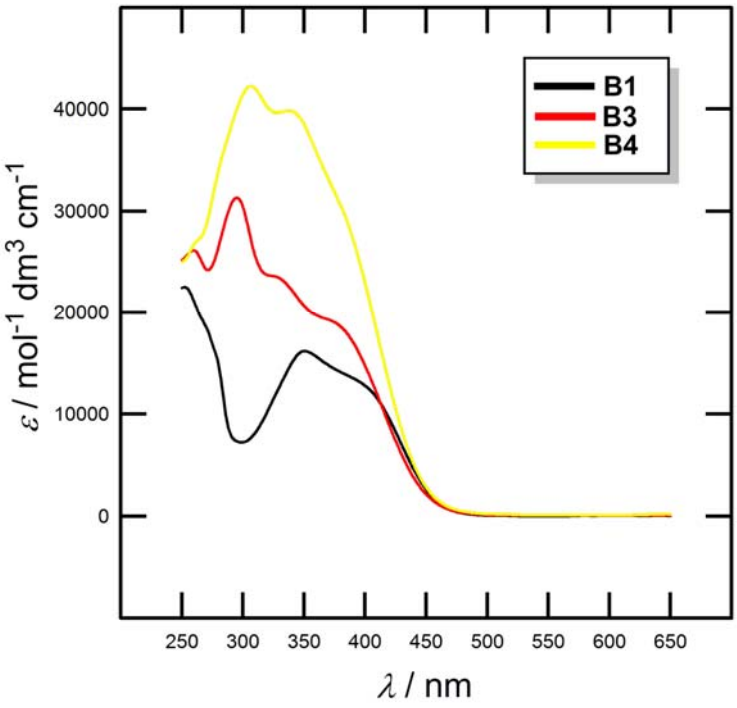

Fig. S3 UV-Vis absorption spectra of chromophores **B1**, **B3** and **B4** measured in CH_2Cl_2 (10^{-5} M).

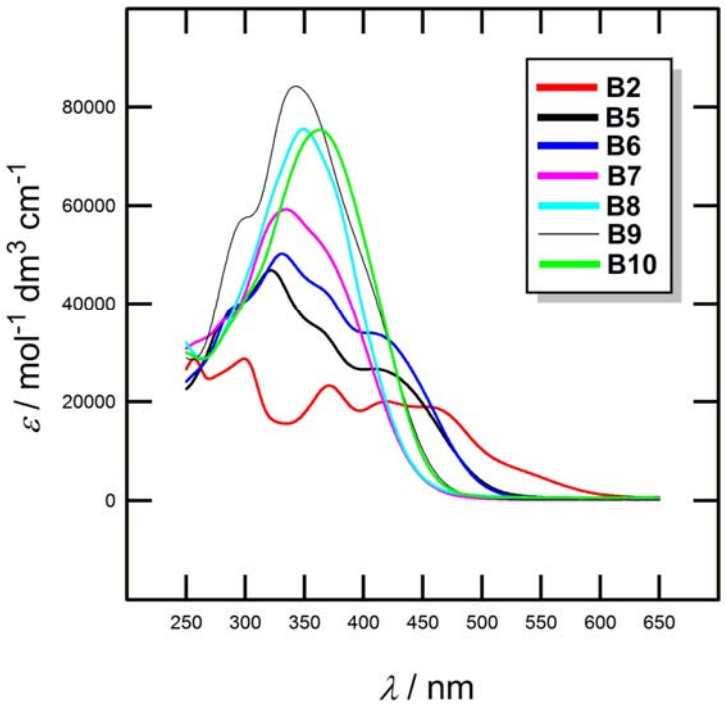

Fig. S4 UV-Vis absorption spectra of chromophores **B2**, **B5**-**B10** measured in CH_2Cl_2 (10^{-5} M).

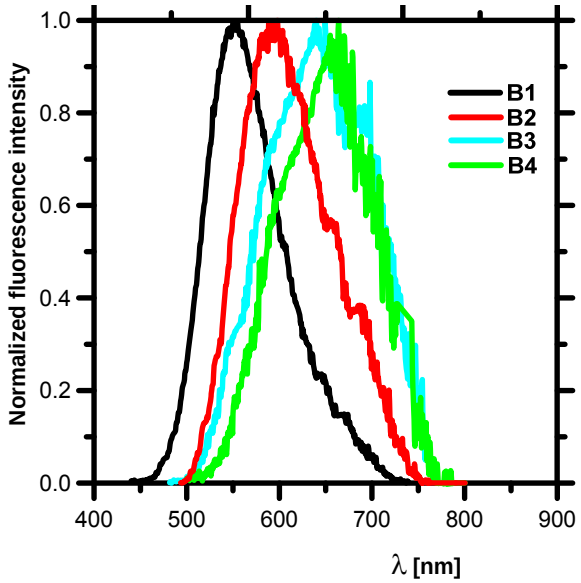

Fig. S5 Fluorescence spectra of chromophores **B1**-**B4** measured in CH_2Cl_2 (10^{-6} M).

6. Data correlations and NLO measurements

The electrochemically measured first oxidation and reduction potentials in DMF were recalculated to the corresponding HOMO and LUMO energies according to the equation: $-E_{HOMO/LUMO} = E^{oF}_{(ox1/red1)} + 4.35$ (Ref.[8]). The electrochemically derived HOMO and LUMO levels and gaps jointly with further optoelectronic parameters of both series of chromophores are presented below in Tables S1 and S2. Both HOMO-LUMO gaps correlates tightly as shown in Fig. S6 and S7.

Nonlinear optical properties of push-pull chromophores **B1**-**B10** were determined experimentally by investigation of the Second Harmonic Generation. The experiment of the SHG was performed for the powdered samples which were oriented by dc-electric field. The studies were performed for the angles which gave the maximal output SHG. A pulsed (pulse duration 15 ns) Nd:YAG laser was used as a fundamental beam for the SHG. A Hamamatsu multiplier together with a Tectronix oscilloscope was served as detectors of the SHG and fundamental time kinetics. Powders of BiB_3O_6 crystallites with known second order susceptibilities were used as reference samples. The measured first hyperpolarizabilities β (SHG) are presented in the Table 5 (main text) as well as in Tables S1 and S2 (below). A sufficiently good correlation has been found between the experimentally measured and AM1-calculated first hyperpolarizabilities β (Fig. S8 and S9). The experimental readouts from the Second Harmonic Generation measurement are shown below. Following the SHG results, there exists some time shift between the temporal position of the fundamental signal and for the SHG. Moreover, some temporal asymmetry in the time delayed SHG. This time delay is most probably a reflection of some trapping levels participating in the process.

Table S1 Optoelectronic parameters of chromophores **B1**-**B10**.

B series	AM1	AM1	AM1	AM1	AM1	EXP	Electrochemistry		
Compd	μ [D]	E_{HOMO} [eV]	E_{LUMO} [eV]	ΔE(AM1) [eV]	β(AM1) [esu×10^{-30}]	β(exp.) [pm V^{-1}]	E (HOMO) [eV]	E (LUMO) [eV]	ΔE(elchem) [eV]
B1	8.56	-8.28	-0.92	7.36	245	0	-5.27	-2.73	2.54
B2	9.74	-8.22	-1.07	7.15	649	0.9	-5.15	-2.87	2.28
B3	9.67	-8.15	-1.18	6.97	375	0	-5.19	-2.94	2.25
B4	10.43	-8.20	-1.31	6.89	681	0	-5.28	-3.07	2.21
B5	10.77	-8.21	-1.47	6.74	809	1.2	-5.16	-3.21	1.95
B6	11.48	-8.16	-1.55	6.61	1263	3.6	-5.24	-3.28	1.96
B7	10.9	-8.18	-1.53	6.65	867	2.1	-5.13	-3.03	2.10
B8	11.3	-8.16	-1.61	6.55	1268	2.8	-5.13	-3.27	1.86
B9	10.89	-8.11	-1.56	6.55	1218	3.2	-5.19	-3.25	1.94
B10	11.78	-8.11	-1.64	6.47	1701	4.9	-5.19	-3.32	1.87

Table S2 Optoelectronic parameters of chromophores **P1**-**P10**.

P series	AM1	AM1	AM1	AM1	AM1	EXP	Electrochemistry		
Compd	μ [D]	E_{HOMO} [eV]	E_{LUMO} [eV]	ΔE(AM1) [eV]	β(AM1) [esu×10^{-30}]	β(exp.) [pm V^{-1}]	E (HOMO) [eV]	E (LUMO) [eV]	ΔE(elchem) [eV]
P1	9.91	-8.40	-1.43	6.97	349	0.53	-5.37	-3.11	2.26
P2	11.89	-8.33	-1.75	6.58	942	1.10	-5.39	-3.48	1.91
P3	9.07	-8.28	-1.78	6.50	408	0.60	-5.16	-3.30	1.86
P4	10.69	-8.23	-1.69	6.54	787	1.10	-5.18	-3.38	1.80
P5	11.49	-8.32	-1.92	6.40	956	1.20	-5.19	-3.61	1.58
P6	11.30	-8.38	-2.01	6.37	1444	1.40	-5.20	-3.66	1.54
P7	-	-	-	-	-	-	-	-	-
P8	-	-	-	-	-	-	-	-	-
P9	11.38	-8.15	-2.00	6.15	1484	3.00	-5.19	-3.65	1.54
P10	11.27	-8.29	-2.07	6.22	1912	3.10	-5.18	-3.68	1.50

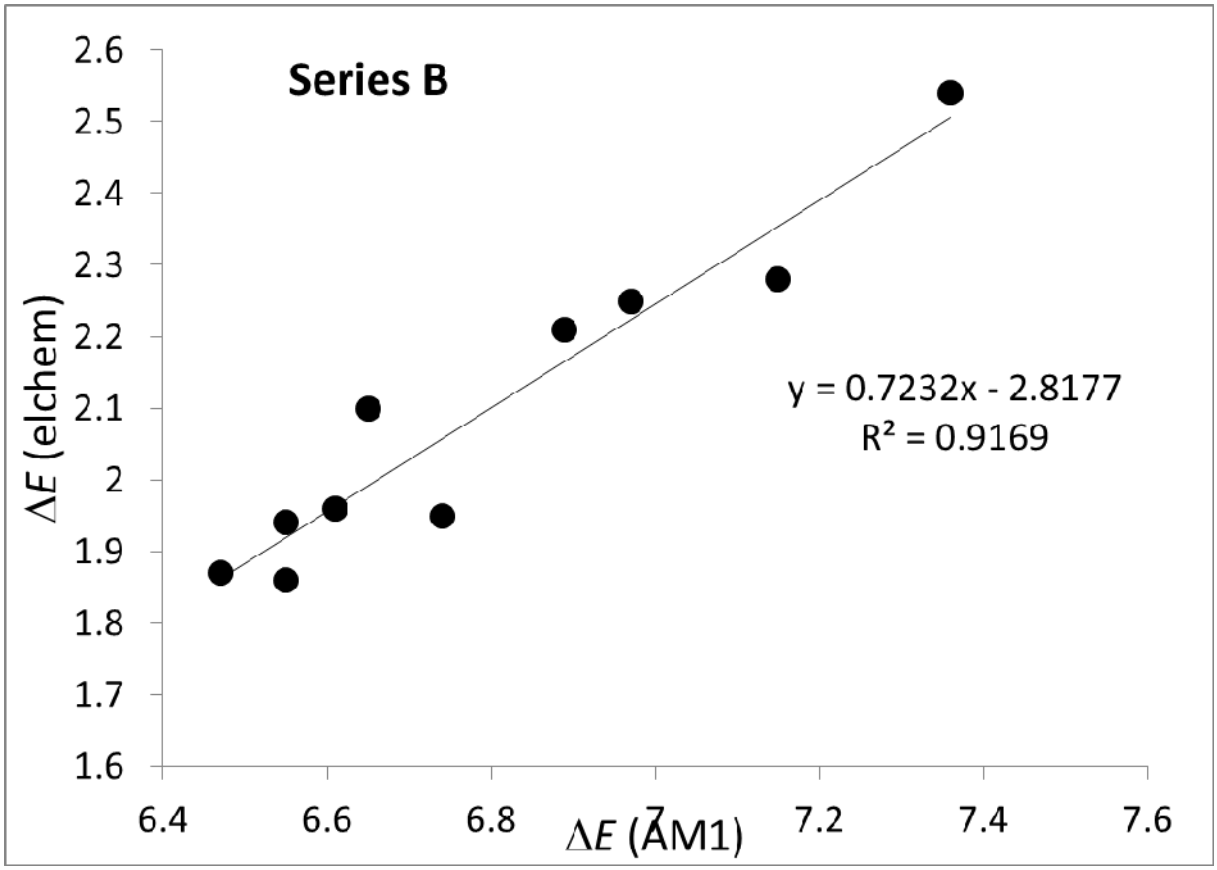

Fig. S6 Correlation of the electrochemical and calculated HOMO-LUMO gaps (series **B**).

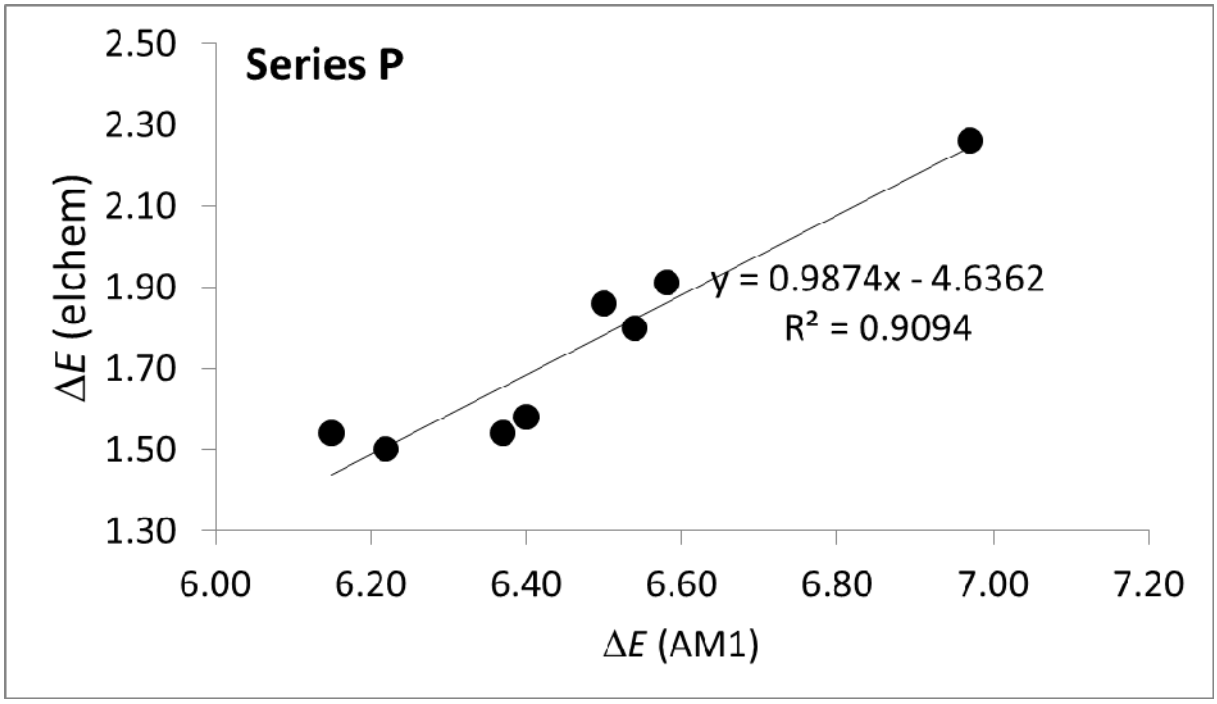

Fig. S7 Correlation of the electrochemical and calculated HOMO-LUMO gaps (series **P**).

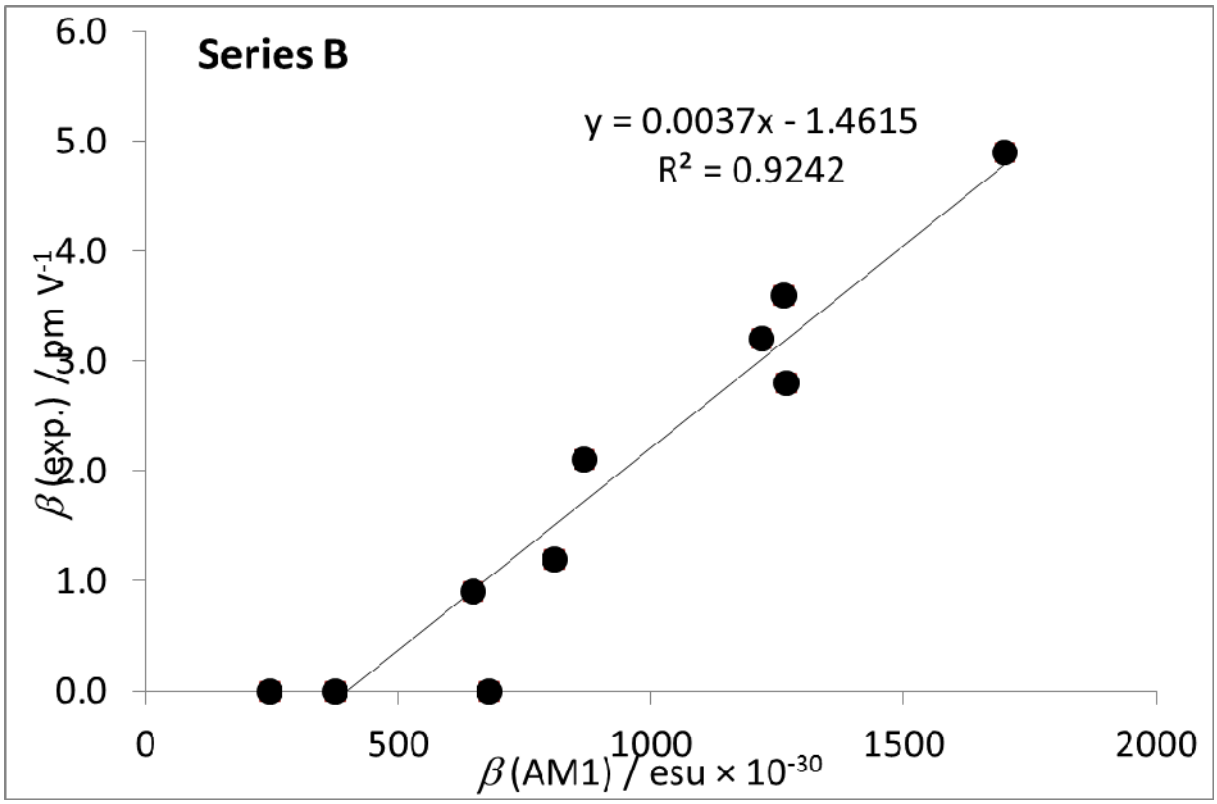

Fig. S8 Experimental SHG values vs. AM1-calculated first hyperpolarizability (series **B**).

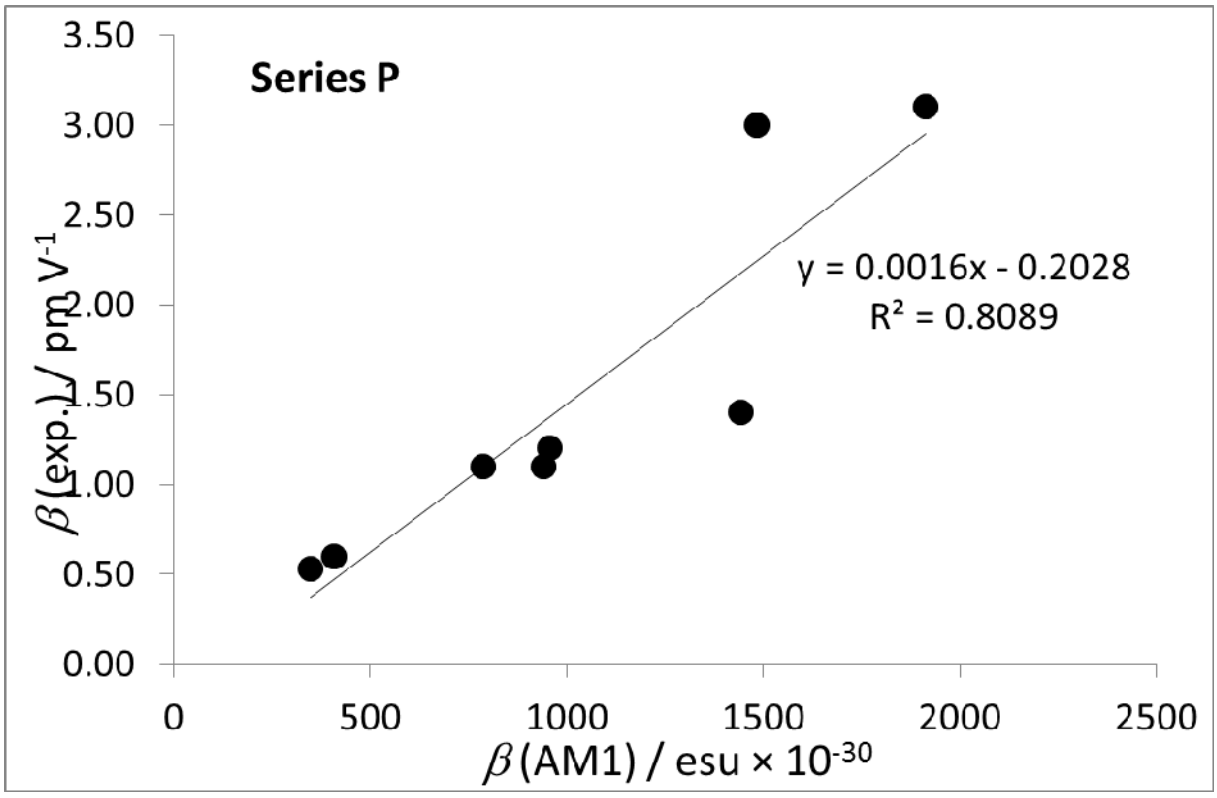

Fig. S9 Experimental SHG values vs. AM1-calculated first hyperpolarizability (series **P**).

7. Experimental readouts from the SHG measurements

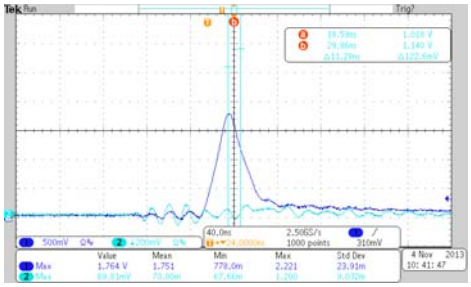

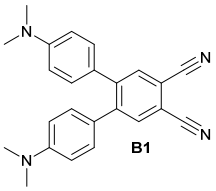

β(exp.) = below noise level

β(AM1) = 245 × 10^{-30} esu

Fig. S10 Experimental readout from the SHG measurements and experimental and theoretical first hyperpolarizability values for **B1**.

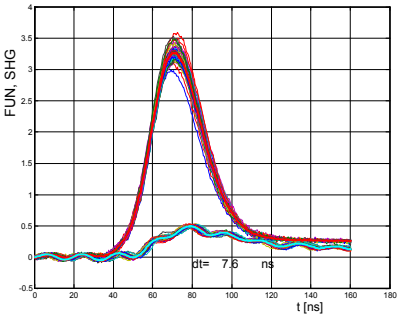

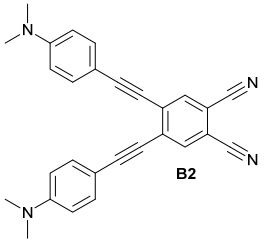

β(exp.) = 0.9 pm V^{-1}

β(AM1) = 649 × 10^{-30} esu

Fig. S11 Experimental readout from the SHG measurements and experimental and theoretical first hyperpolarizability values for **B2**.

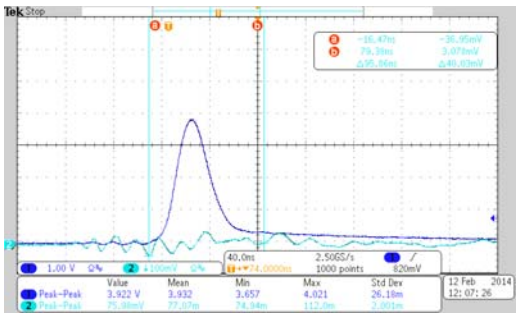

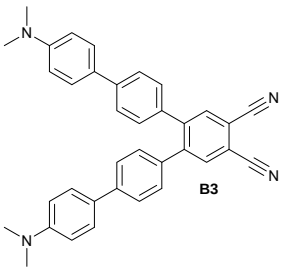

β(exp.) = below noise level

β(AM1) = 375 × 10^{-30} esu

Fig. S12 Experimental readout from the SHG measurements and experimental and theoretical first hyperpolarizability values for **B3**.

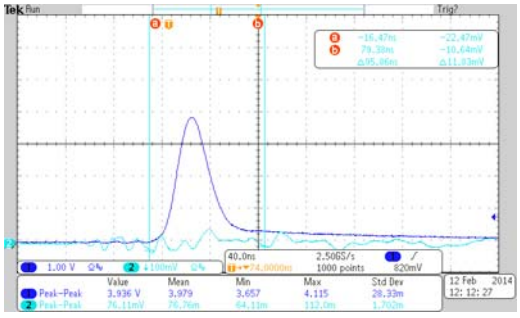

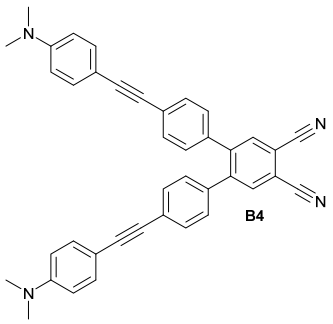

β(exp.) = below noise level

β(AM1) = 681 × 10^{-30} esu

Fig. S13 Experimental readout from the SHG measurements and experimental and theoretical first hyperpolarizability values for **B4**.

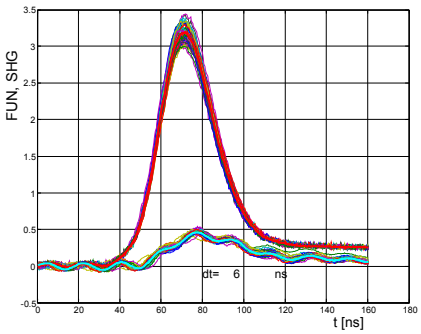

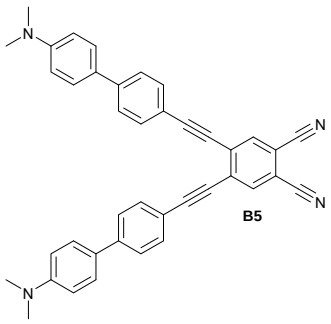

β(exp.) = 1.2 pm V^{-1}

β(AM1) = 809 $\times$ 10^{-30} esu

Fig. S14 Experimental readout from the SHG measurements and experimental and theoretical first hyperpolarizability values for **B5**.

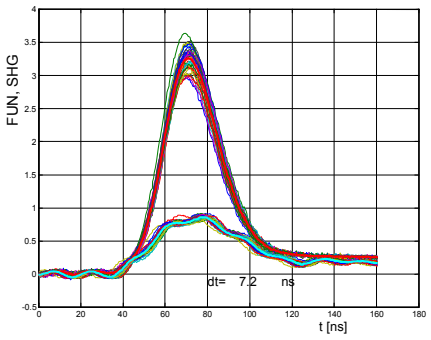

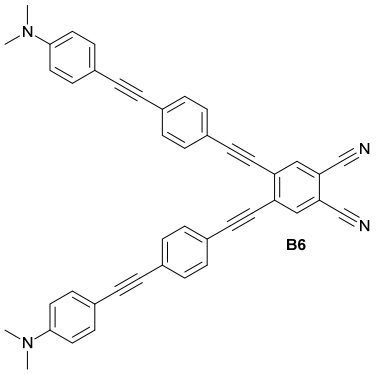

β(exp.) = 3.6 pm V^{-1}

β(AM1) = 1263 $\times$ 10^{-30} esu

Fig. S15 Experimental readout from the SHG measurements and experimental and theoretical first hyperpolarizability values for **B6**.

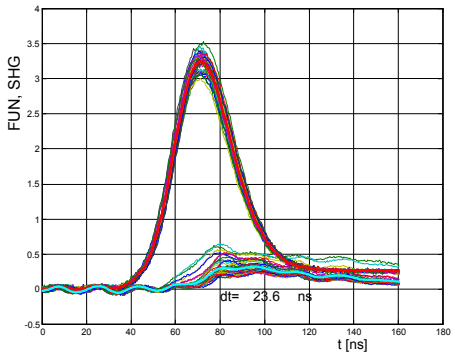

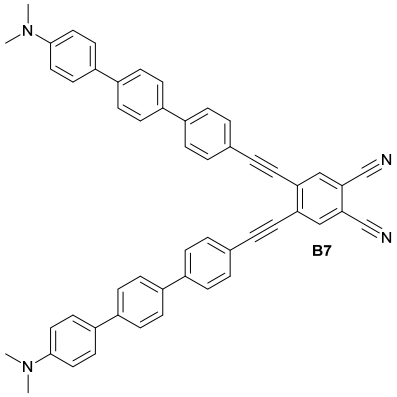

β(exp.) = 2.1 pm V^{-1}

β(AM1) = 867 $\times$ 10^{-30} esu

Fig. S16 Experimental readout from the SHG measurements and experimental and theoretical first hyperpolarizability values for **B7**.

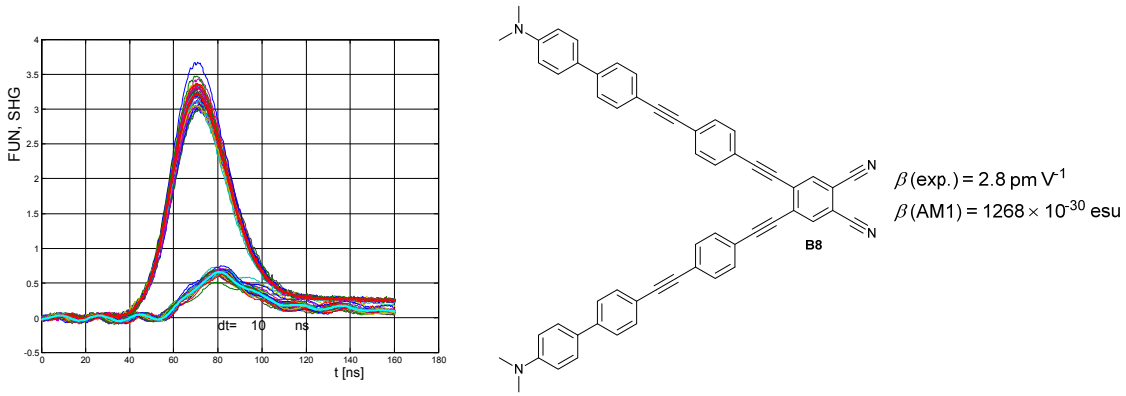

Fig. S17 Experimental readout from the SHG measurements and experimental and theoretical first hyperpolarizability values for **B8**.

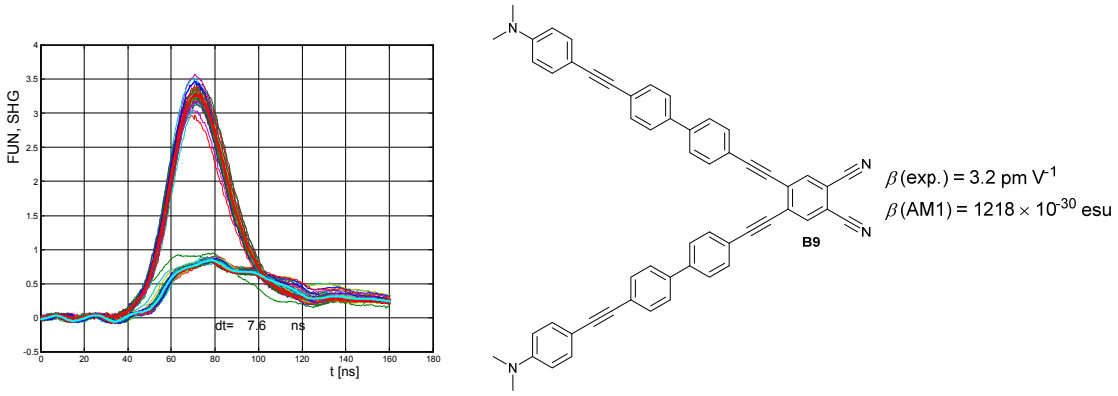

Fig. S18 Experimental readout from the SHG measurements and experimental and theoretical first hyperpolarizability values for **B9**.

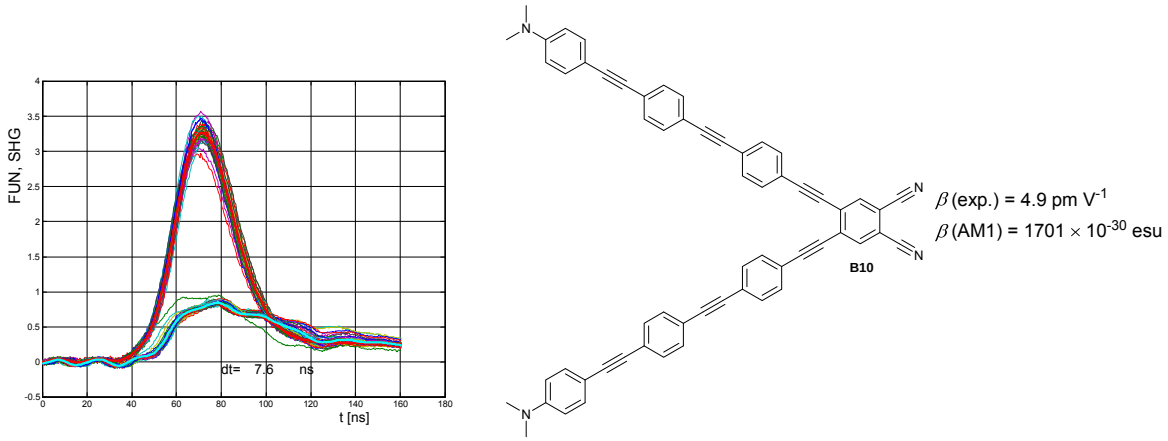

Fig. S19 Experimental readout from the SHG measurements and experimental and theoretical first hyperpolarizability values for **B10**.

8. HOMO and LUMO localizations

The following figures have been derived from AM1 calculations.

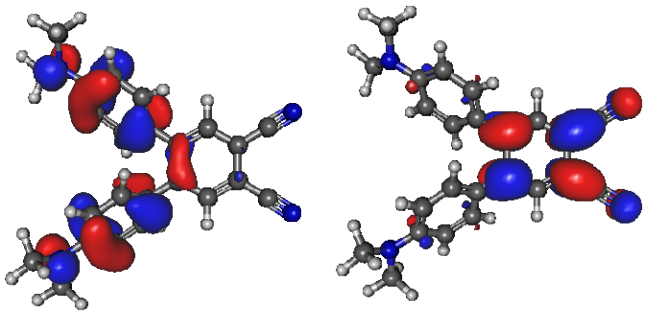

Fig. S20 The HOMO (left) and LUMO (right) localizations in **B1**.

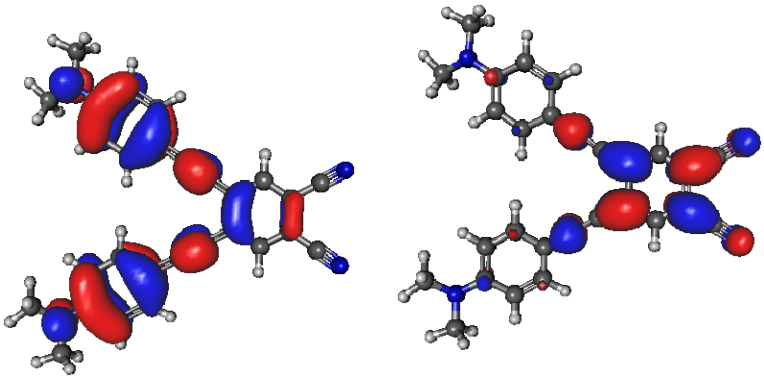

Fig. S21 The HOMO (left) and LUMO (right) localizations in **B2**

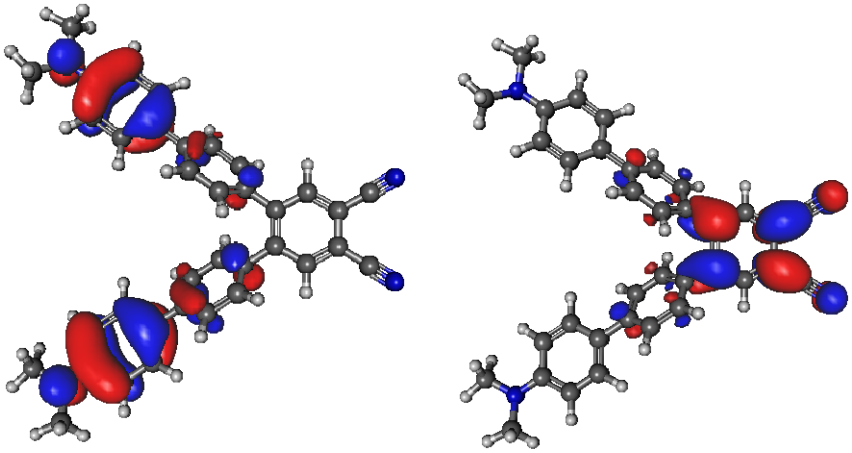

Fig. S22 The HOMO (left) and LUMO (right) localizations in **B3**.

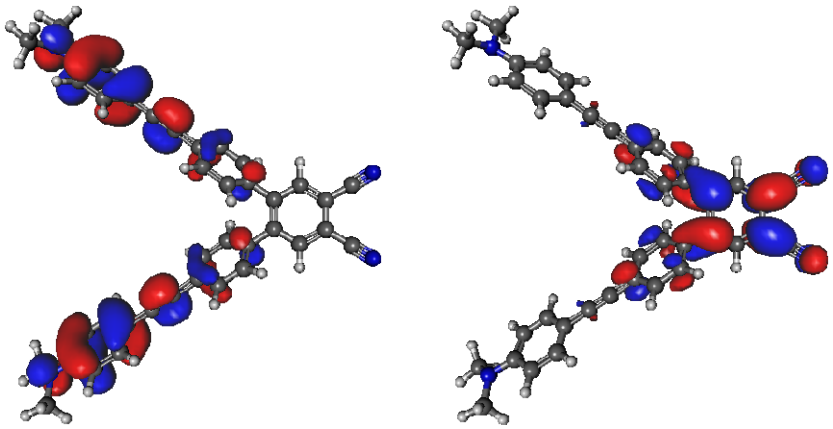

Fig. S23 The HOMO (left) and LUMO (right) localizations in **B4**.

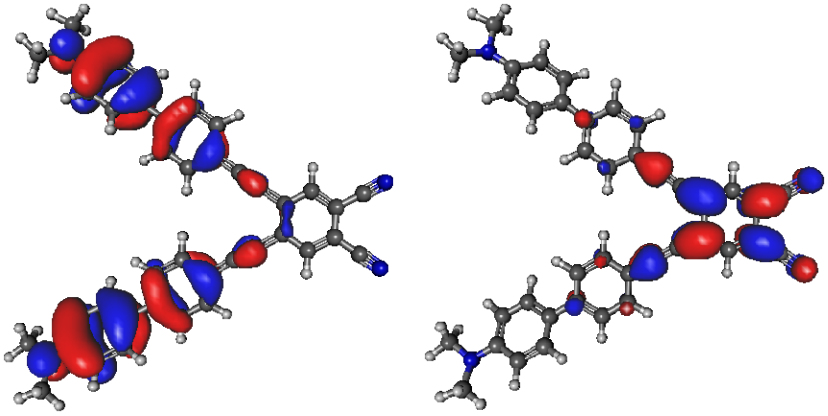

Fig. S24 The HOMO (left) and LUMO (right) localizations in **B5**.

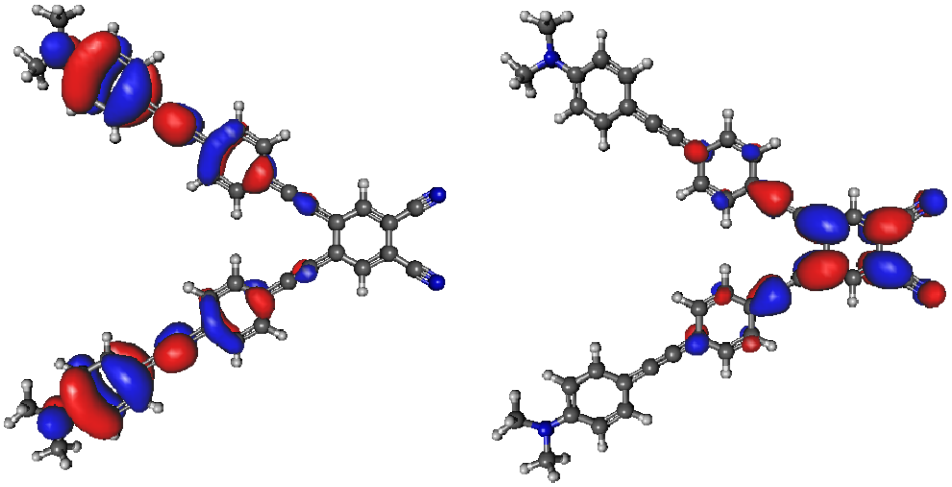

Fig. S25 The HOMO (left) and LUMO (right) localizations in **B6**.

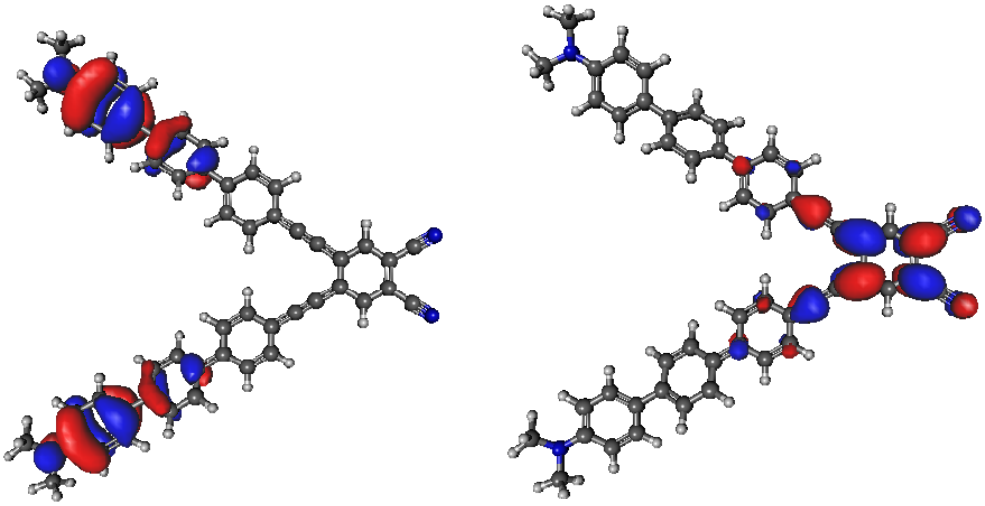

Fig. S26 The HOMO (left) and LUMO (right) localizations in **B7**.

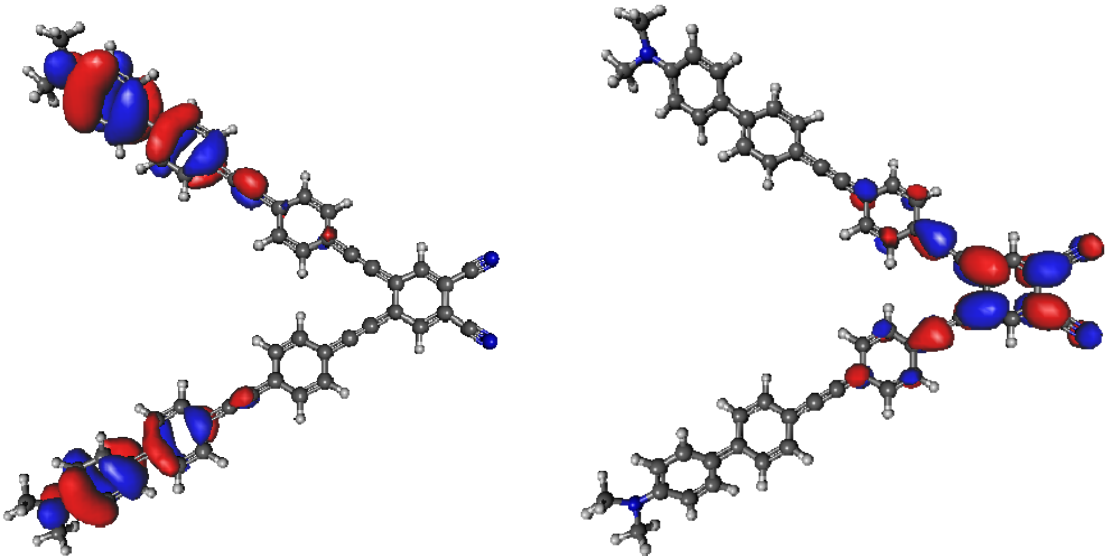

Fig. S27 The HOMO (left) and LUMO (right) localizations in **B8**.

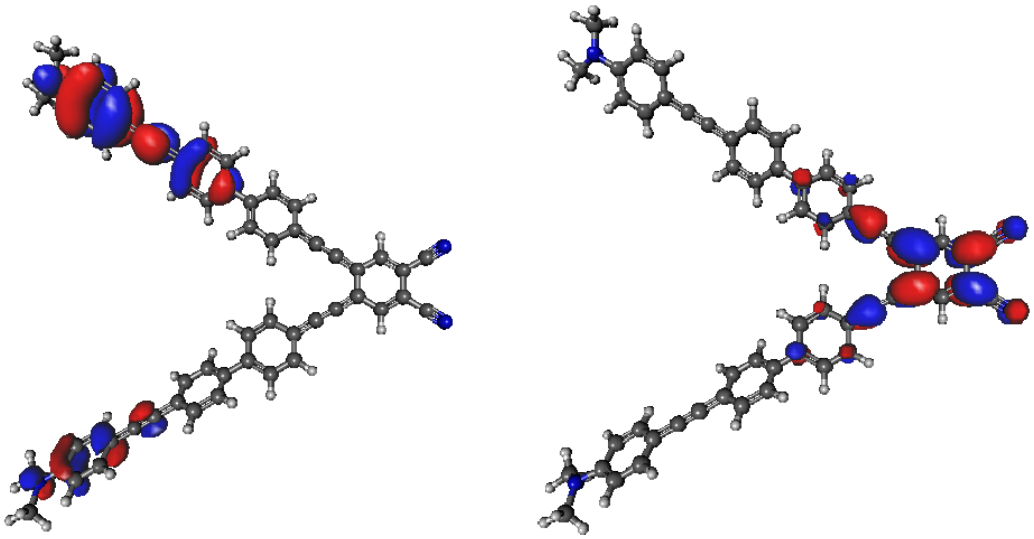

Fig. S28 The HOMO (left) and LUMO (right) localizations in **B9**.

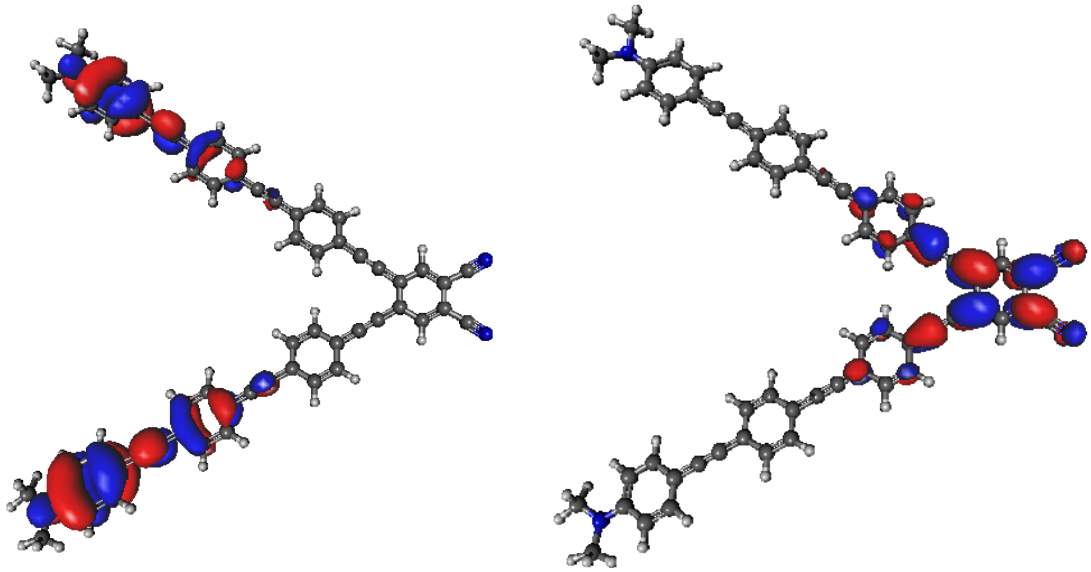

Fig. S29 The HOMO (left) and LUMO (right) localizations in **B10**.

9. ^{1}H and ^{13}C NMR spectra of target compounds B1-B10

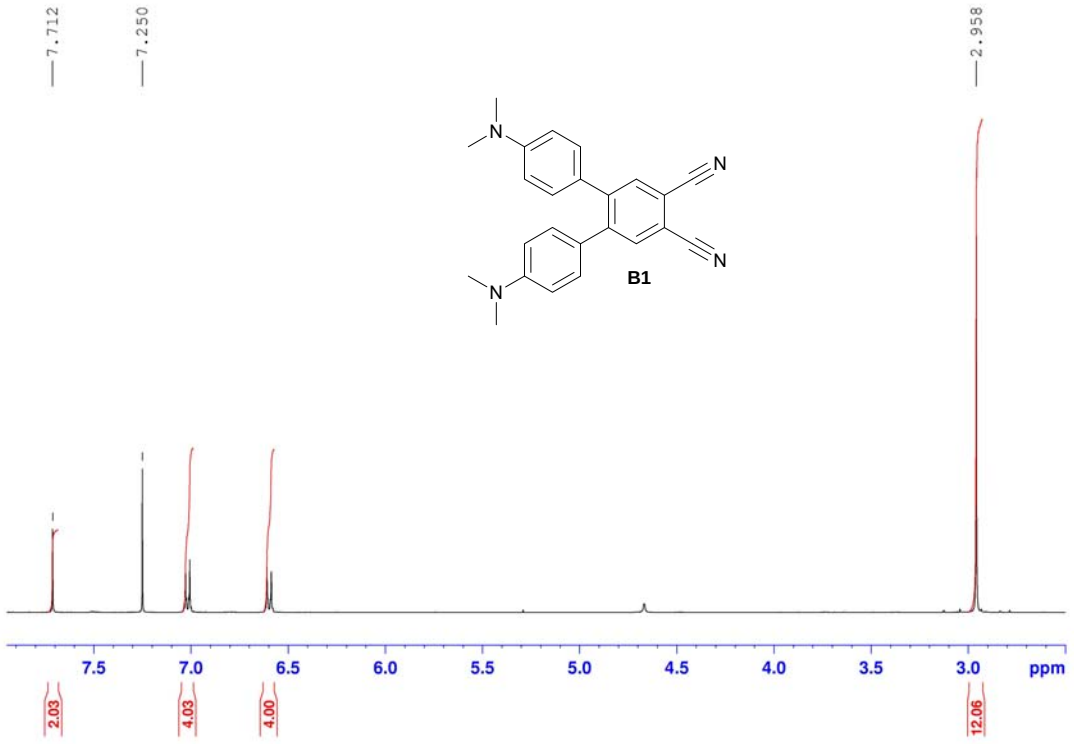

Fig. S30 ^{1}H NMR spectrum of chromophore **B1** ($CDCl_3$, 400 MHz, 25 °C).

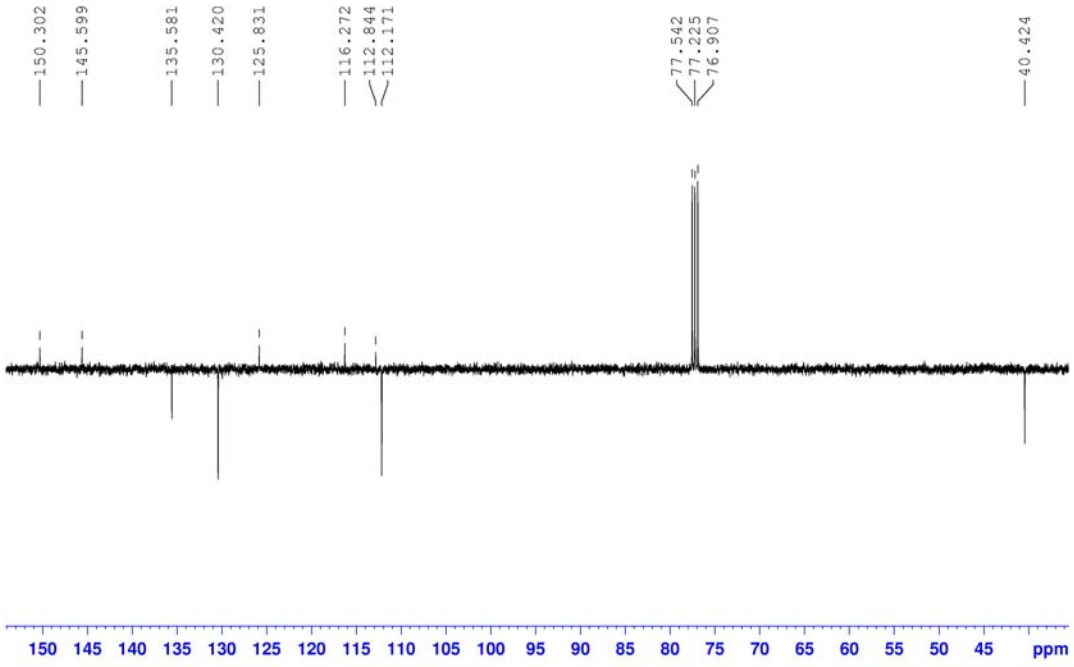

Fig. S31 ^{13}C NMR APT spectrum of chromophore **B1** ($CDCl_3$, 100 MHz, 25 °C).

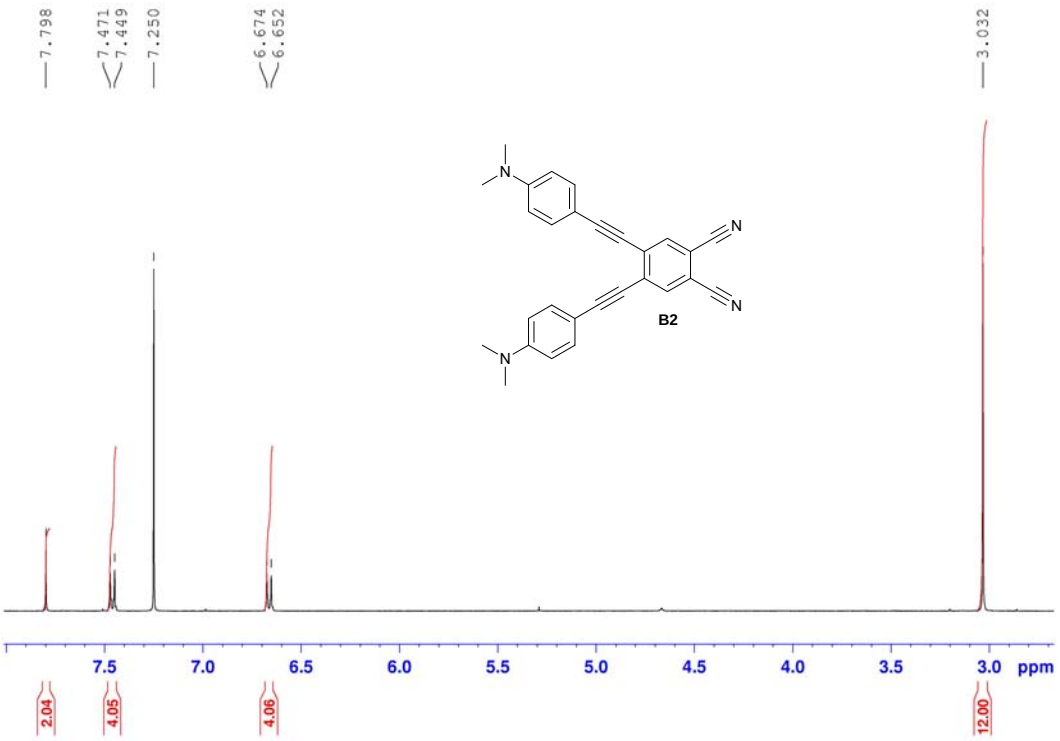

Fig. S32 ^{1}H NMR spectrum of chromophore **B2** ($CDCl_3$, 400 MHz, 25 °C).

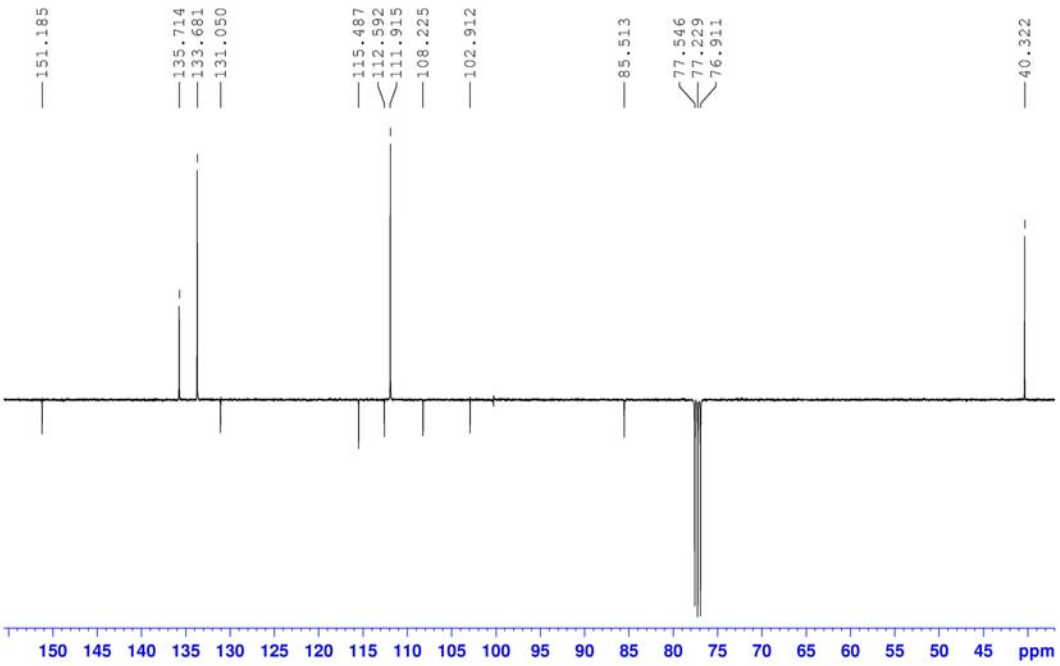

Fig. S33 ^{13}C NMR APT spectrum of chromophore **B2** ($CDCl_3$, 100 MHz, 25 °C).

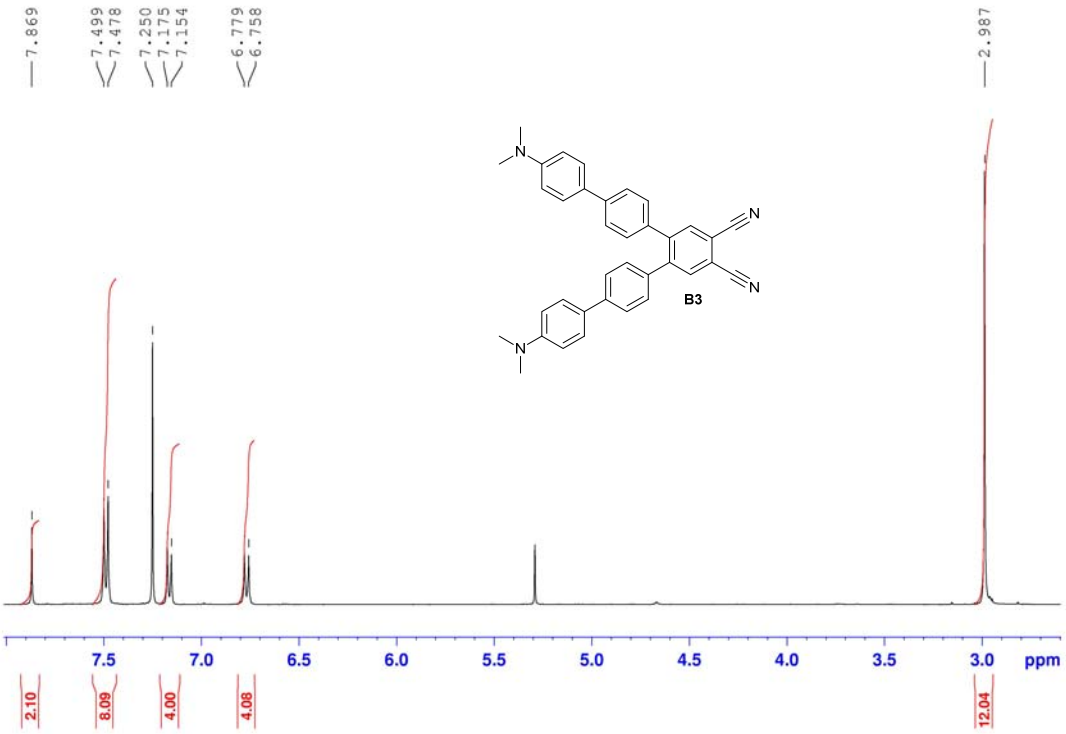

Fig. S34 ^{1}H NMR spectrum of chromophore **B3** ($CDCl_3$, 400 MHz, 25 °C).

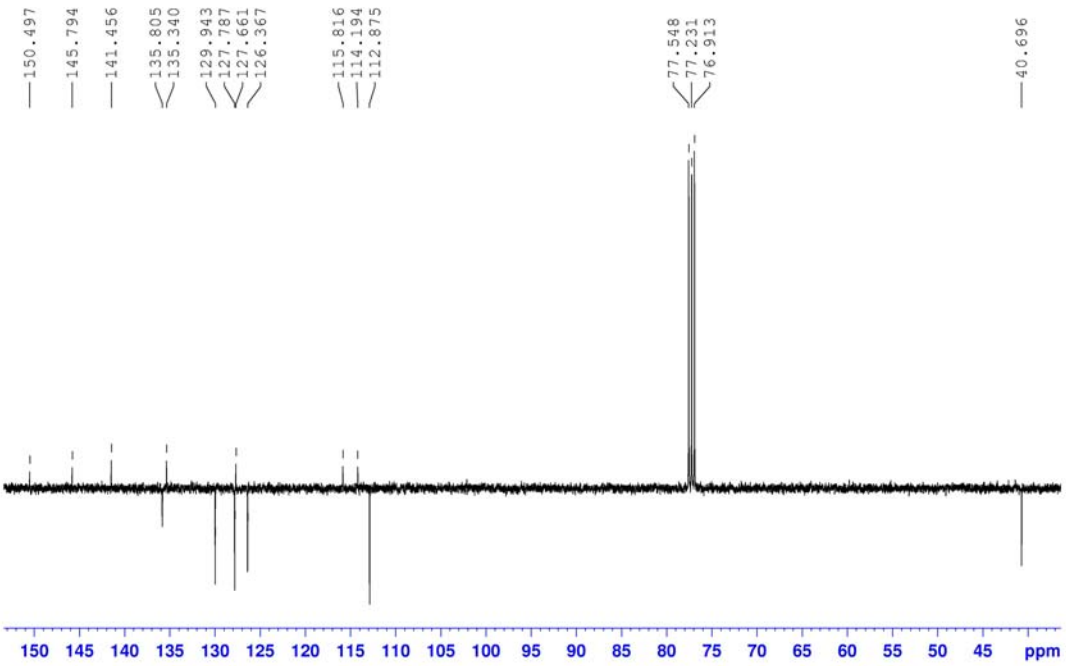

Fig. S35 ^{13}C NMR APT spectrum of chromophore **B3** ($CDCl_3$, 100 MHz, 25 °C).

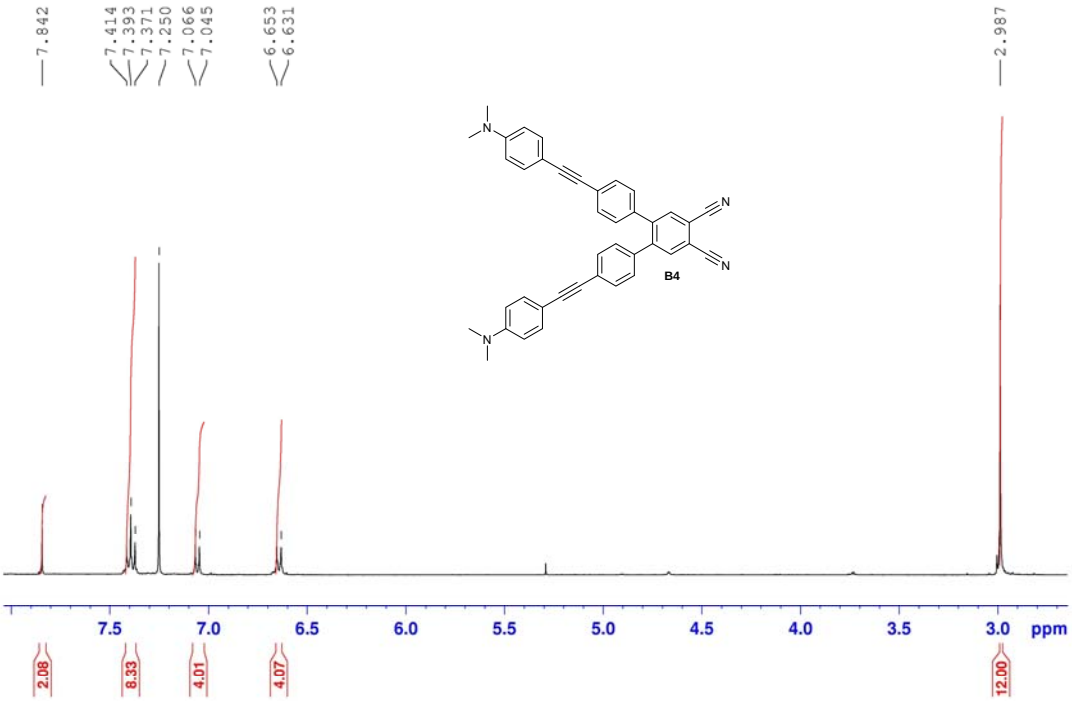

Fig. S36 ^{1}H NMR spectrum of chromophore **B4** ($CDCl_3$, 400 MHz, 25 °C).

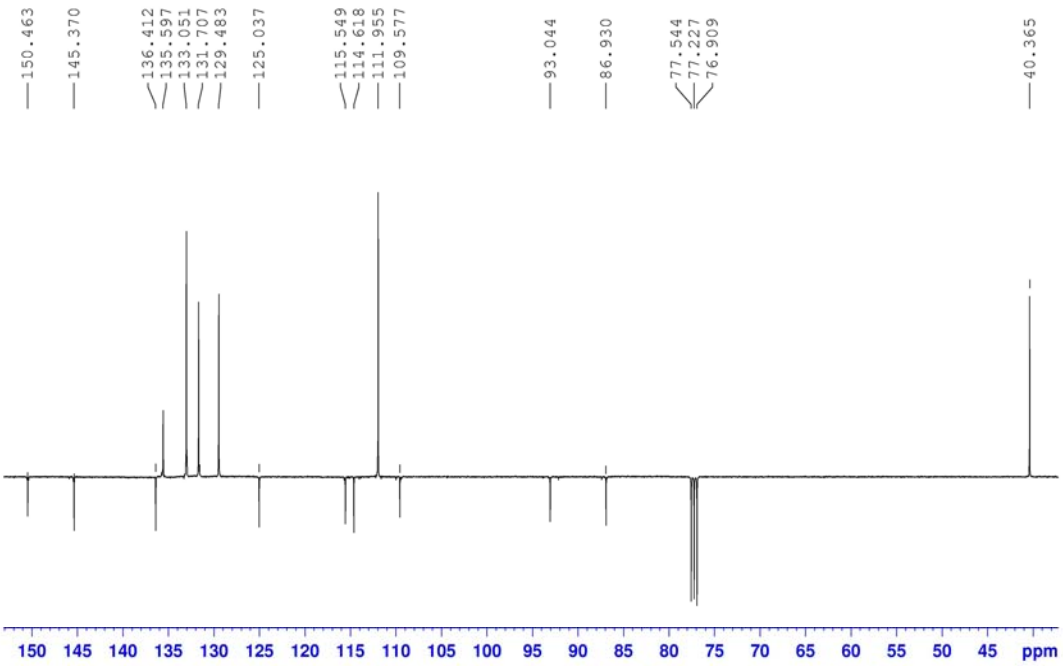

Fig. S37 ^{13}C NMR APT spectrum of chromophore **B4** ($CDCl_3$, 100 MHz, 25 °C).

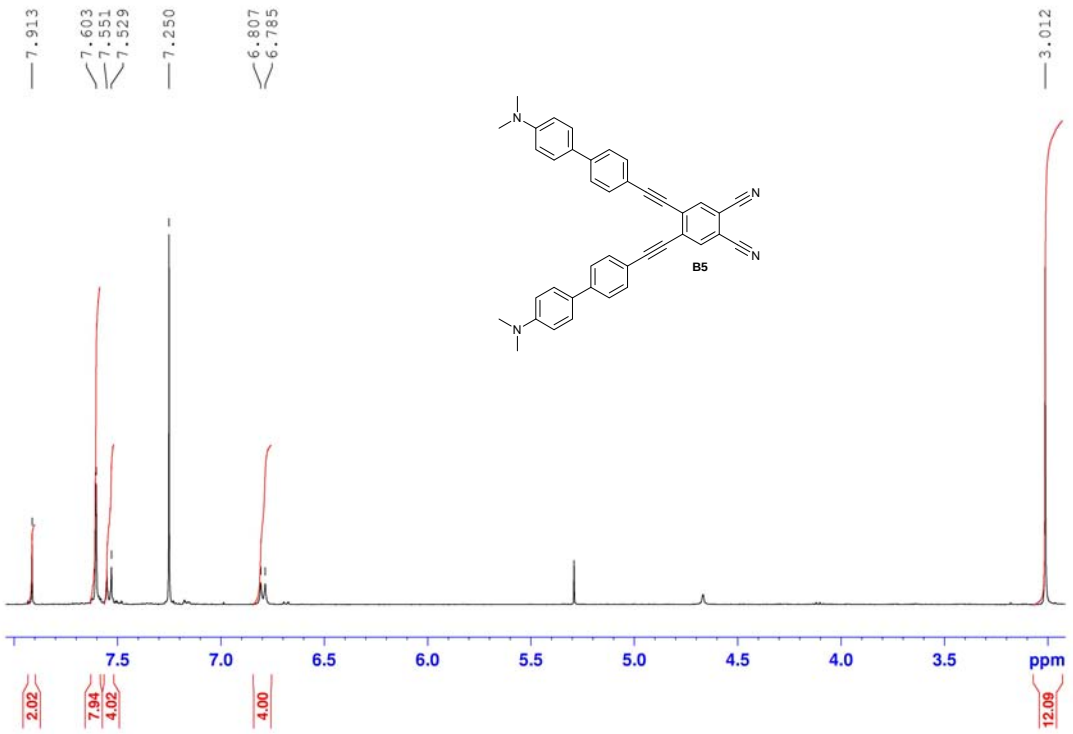

Fig. S38 ^{1}H NMR spectrum of chromophore **B5** ($CDCl_3$, 400 MHz, 25 °C).

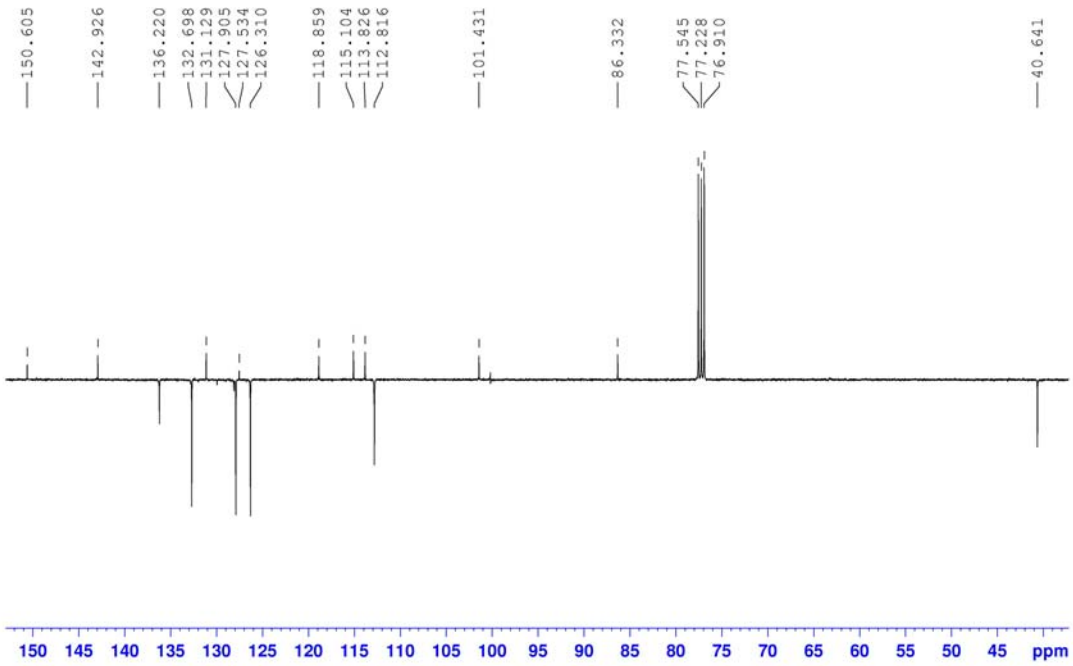

Fig. S39 ^{13}C NMR APT spectrum of chromophore **B5** ($CDCl_3$, 100 MHz, 25 °C).

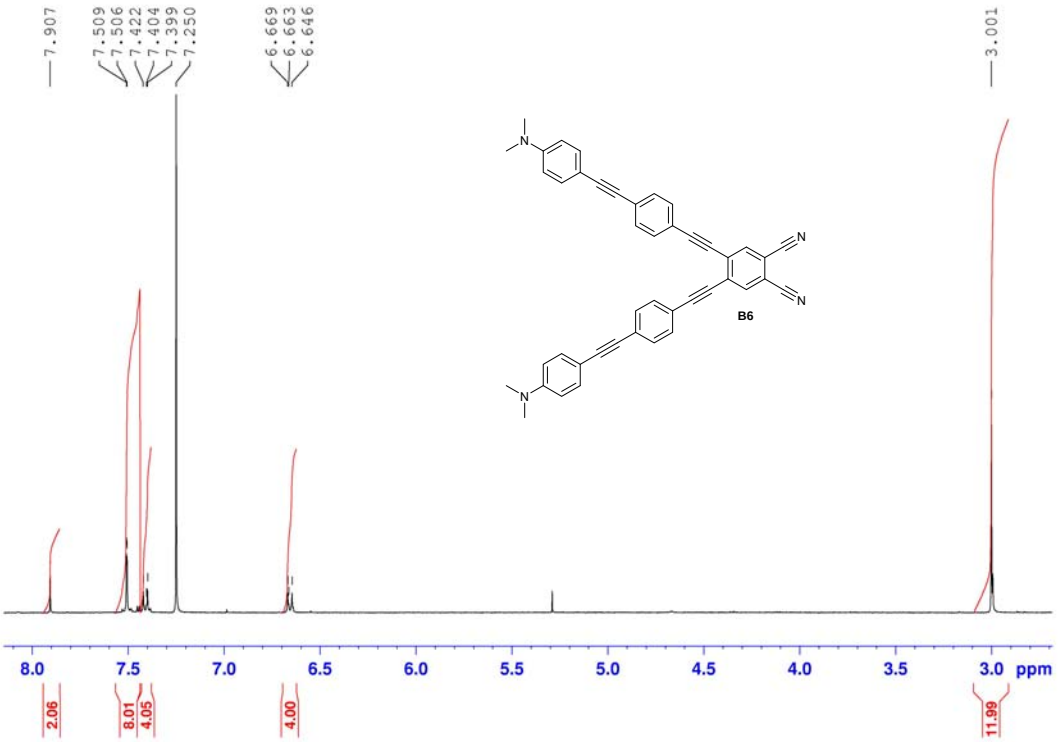

Fig. S40 ^{1}H NMR spectrum of chromophore **B6** ($CDCl_3$, 400 MHz, 25 °C).

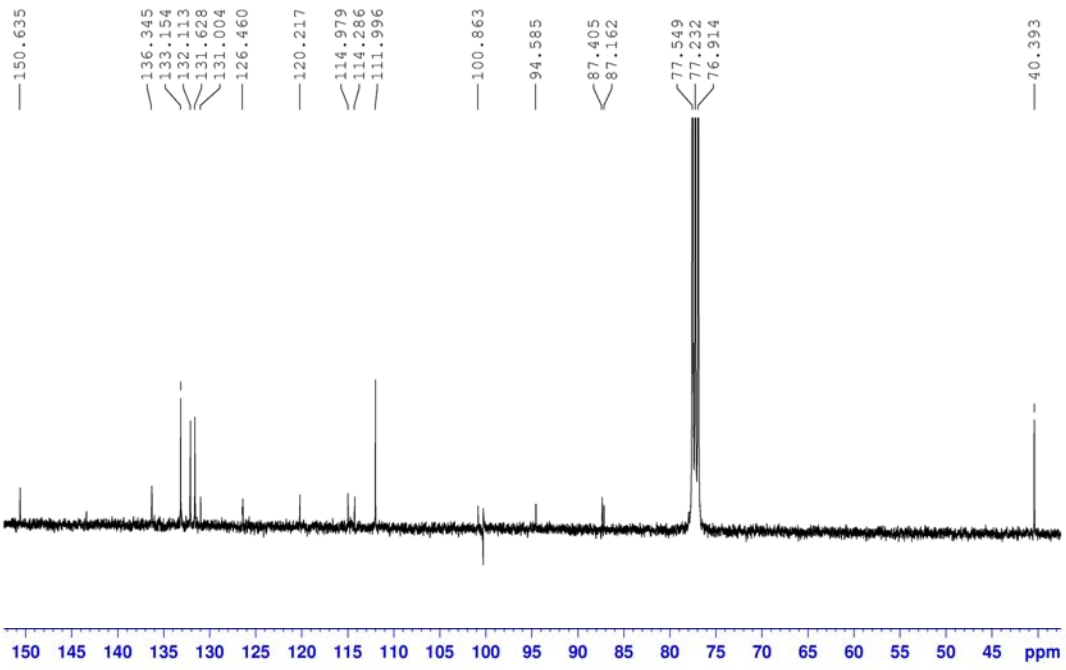

Fig. S41 ^{13}C NMR APT spectrum of chromophore **B6** ($CDCl_3$, 100 MHz, 25 °C).

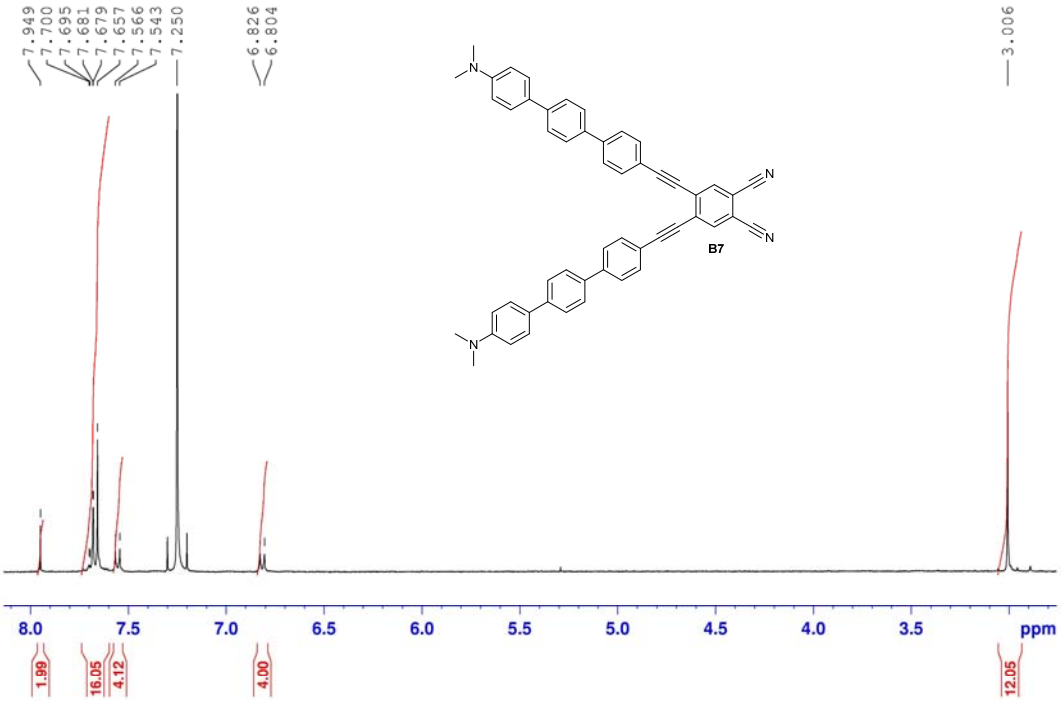

Fig. S42 ^{1}H NMR spectrum of chromophore **B7** ($CDCl_3$, 400 MHz, 25 °C, 160 scans).

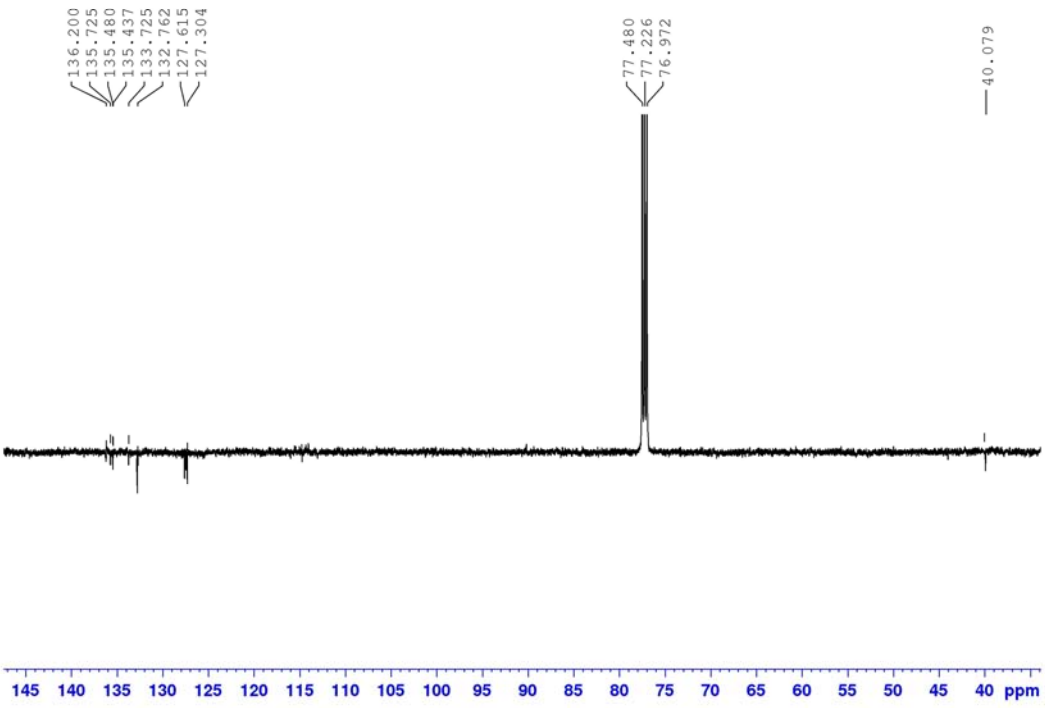

Fig. S43 ^{13}C NMR APT spectrum of chromophore **B7** ($CDCl_3$, 125 MHz, 25 °C, 16.000 scans).

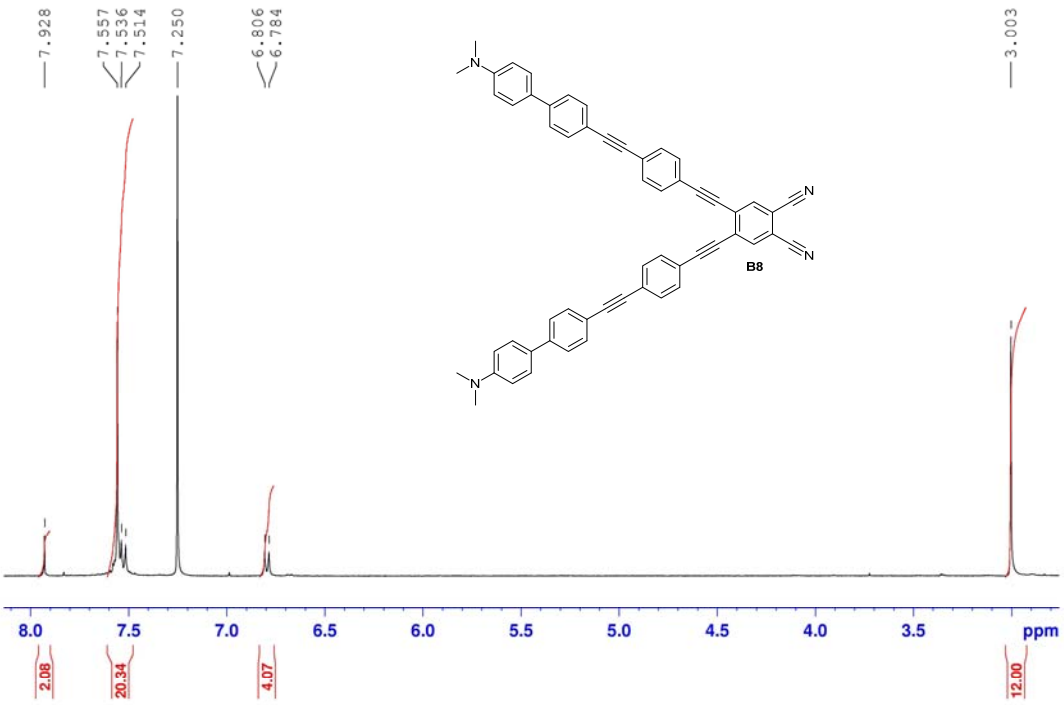

Fig. S44 ^{1}H NMR spectrum of chromophore **B8** ($CDCl_3$, 400 MHz, 25 °C).

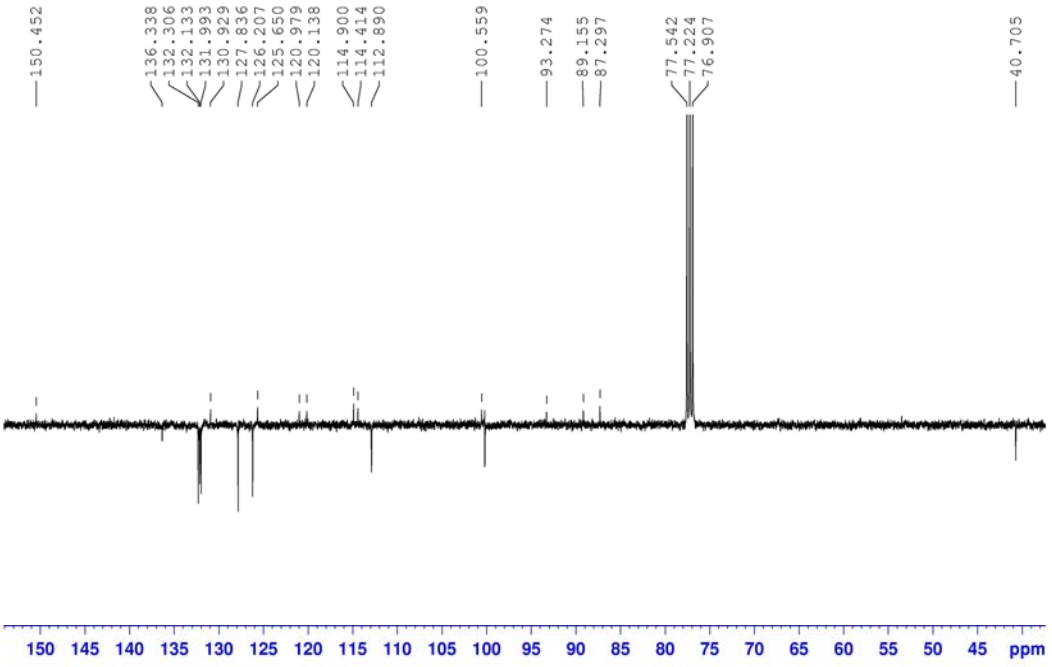

Fig. S45 ^{13}C NMR APT spectrum of chromophore **B8** ($CDCl_3$, 100 MHz, 25 °C).

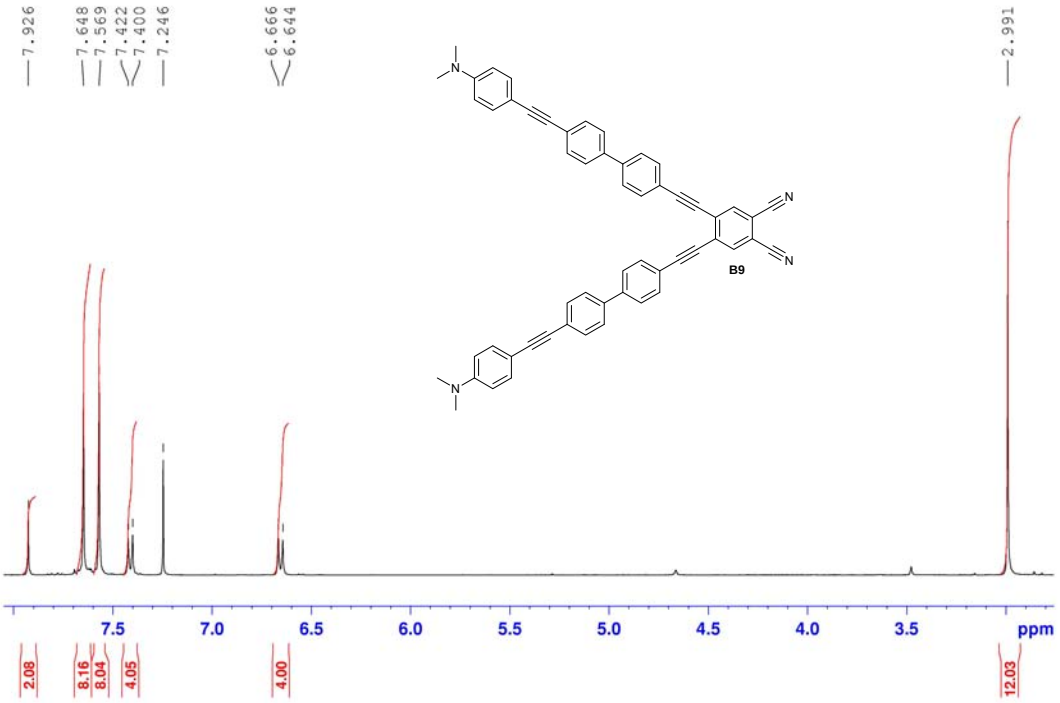

Fig. S46 ^{1}H NMR spectrum of chromophore **B9** ($CDCl_3$, 400 MHz, 25 °C).

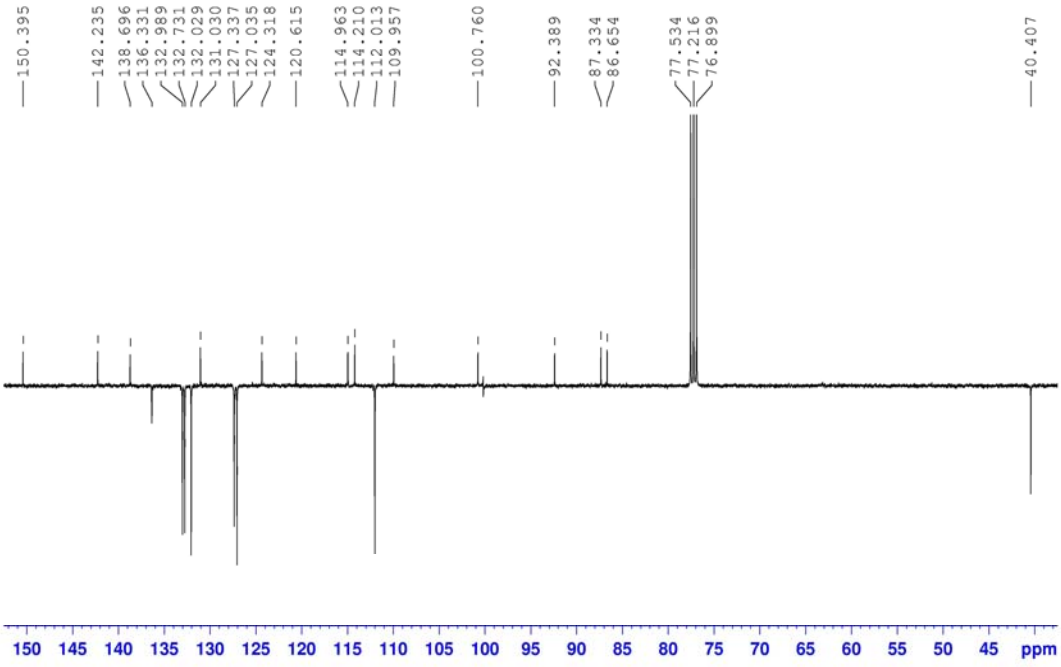

Fig. S47 ^{13}C NMR APT spectrum of chromophore **B9** ($CDCl_3$, 100 MHz, 25 °C).

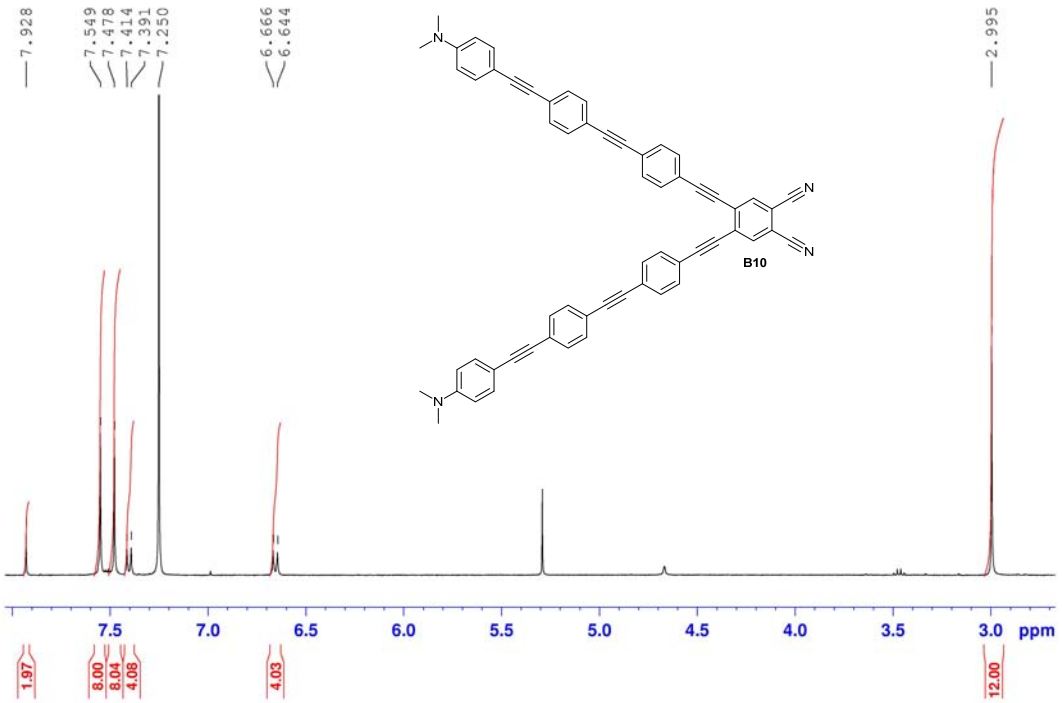

Fig. S48 ^{1}H NMR spectrum of chromophore **B10** ($CDCl_3$, 400 MHz, 25 °C).

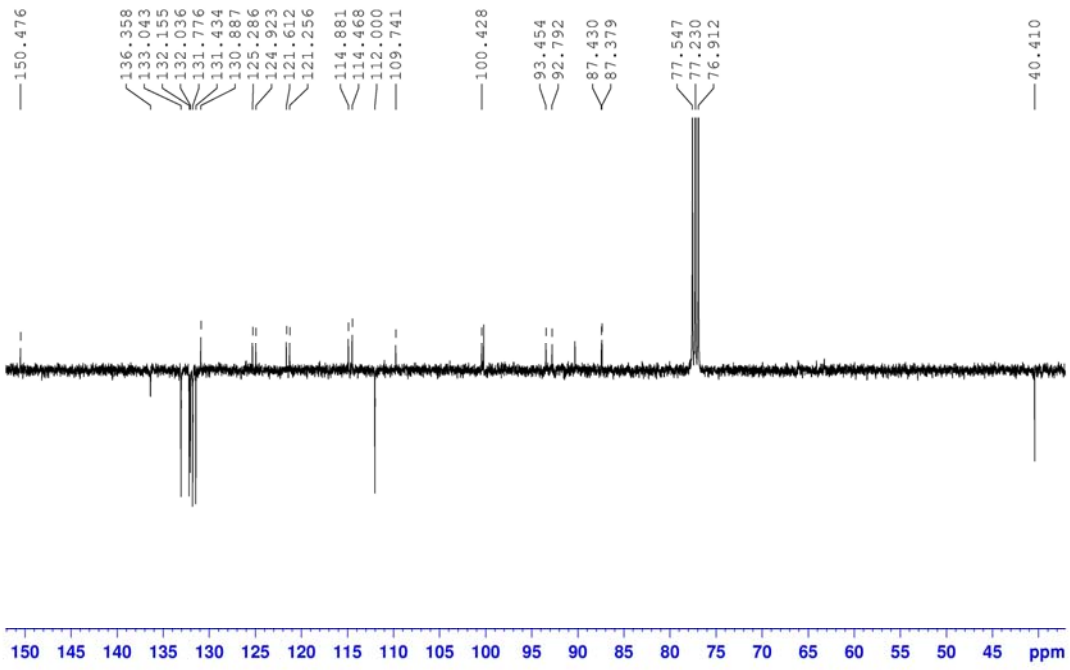

Fig. S49 ^{13}C NMR APT spectrum of chromophore **B10** ($CDCl_3$, 100 MHz, 25 °C).

10. References

1 S. L. Bondarev, V. N. Knyukshto, V. I. Stepuro, A. P. Stupak and A. A. Turban. *J. Appl. Spec.*, 2004, **71**, 194.

2 G. Jones II and M. A. Rahman, *J. Phys. Chem.* 1994, **98**,13028.

3 D. S. Terekhov, K. J. M. Nolan, C. R. McArthur and C. C. Leznoff, *J. Org. Chem.*, 1996, **61**, 3034-3040.

4 Z. Otwinowski, W. Minor, W., *Methods in Enzymology,* 1997, **276**, 307.

5 P. Coppens, in *Crystallographic Computing,* Eds. F. R. Ahmed, S. R. Hall and C. P. Huber, Munksgaard, Copenhagen, 1970, pp. 255–270.

6 A. Altomare, G. Cascarano, C. Giacovazzo and A. Guagliardi, *J. Appl. Crystallogr.,* 1993, **26**, 343.

7 SHELXL-97*,* G. M. Sheldrick, University of Göttingen, Göttingen, 1997.

8 A. Isse and A. Gennaro, *J. Phys. Chem. B*, 2010, **114**, 7894-7899.